DOI: 10.1111/bph.16112



# Neuropharmacology

## OC021 | Novel mechanisms of GW117 in antidepressant and anxiolytic-like activity

**Zengliang Jin; Yaqi Yang**
*Capital Medical University*

**Introduction**

Major depressive disorder (MDD) is a worsening problem worldwide. GW117 is a novel MT1/MT2 receptor agonist and 5-HT2C receptor antagonist of multitarget antidepressant that we previously identified. Here, we further investigated the mechanism of anxiolytic and antidepressant effects of GW117 and its potential to improve sleep.

**Methods**

We used a modified chronic unpredictable mild stress (CUMS) model to induce depression-like behavior and circadian rhythm disturbance in rats and explored changes in clock genes, sleep homeostasis markers and neurogenesis by real-time quantitative PCR, ELISA, western blotting and immunofluorescence staining. We investigated the ability and mechanism of GW117 to normalize CUMS-induced abnormal behavior and regulate circadian rhythm through several animal behavioral tests, EEG and EMG monitoring and molecular techniques described above.

**Results**

GW117 significantly increased the sucrose preference rate of CUMS rats in sucrose preference tests. GW117 effectively enhanced the total distance and the number of rearing and crossings, and increased residence time and number of entries in the central zone of open field, decreased fecal pellets. GW117 significantly decreased the immobility time of CUMS rats in forced swimming test, and reduced the feeding latency in the novelty- suppressed feeding test, increased the number of electro shock drinking episodes of CUMS rats in Vogel drinking conflict test. GW117 significantly prolonged the dwell time of rats in the open arm, increased the frequency of rats entering the open arm in O-maze assay. GW117 significantly increased the mRNA levels of Clock, Per1, Per2, Cry1, Cry2, Bmal1 and Npas2 in the hypothalamus of CUMS rats, and increased the level of 5-HT and melatonin and decreased the levels of cortisol in the serum of CUMS rats. GW117 significantly increased the expression of BDNF and GFAP in the hippocampus of CUMS rats, and increased the amount of BrdU+/Dcx+ and BrdU+/GFAP+ in the SGZ region. And GW117 can activate the Wnt/β-catenin signaling pathway, which significantly increased the levels of β-catenin, c-Myc and cyclin D1 in hippocampal neurons of CUMS rats.

**Conclusions**

All results suggest that GW117 as a novel antidepressant has stronger anxiolytic and antidepressant effects and can improve circadian rhythms, which is the result of a synergistic effect of melatonin system-mediated regulation of circadian rhythms and promotion of hippocampal neurogenesis.

## OC022 | Pterostilbene attenuates Diabetes induced Depression in Wistar rats by its anti-inflammatory action and ameliorating HPA axis

**Ms Rashmi Patil; Urmila Aswar**
*Poona college of Pharmacy, Bharati Vidyapeeth (Deemed to be) University*

**Introduction**

Long-term hyperglycemia in diabetes deregulates the cerebral metabolism which consequently leads to the development of psychiatric comorbidities. The probability of major depressive disorder is almost twice in type 2 diabetes mellitus (T2DM) as compared to general population [1]. HPA axis dysregulation and inflammation are major contributory factors for the development of depression due to insulin resistance [2]. Pterostilbene (PTE), a dimethylated analog of resveratrol is naturally found in blueberries, grapes, and red wood. It is reported to exhibit antioxidant, neuroprotective, hypolipidemic, anti-inflammatory and hypoglycaemic effects but is not studied for diabetes-induced depression (DID) [3]. Present study evaluated the effects of PTE on depression-like behaviour in male Wistar rats with T2DM.

[Correction added on 31 October 2023, after first online publication: additional abstracts P0774 and P1146 have been added at the end of this supplement issue (pages 1426-1428).]

  

BJP BRITISH PHARMACOLOGICAL SOCIETY

### Methods

T2DM was induced by single dose administration of nicotinamide (NA; 75 mg/kg) and streptozotocin (STZ; 55 mg/kg). Post 72 hours, rats with blood glucose (BG) level >220 mg/dL were deemed diabetic, which were left untreated for 21 days. On day 21, forced swim test (FST) was conducted for the confirmation of DID. These rats were randomized and treated orally with PTE (10, 20 and 40 mg/kg), metformin (500 mg/kg) or fluoxetine (10 mg/kg) for 28 days. At the end of the treatment, sucrose preference test (SPT) and open field test (OFT) was performed to assess the depression in rats. The rats were then euthanized under anaesthesia to collect the blood for measuring the lipid profile (cholesterol, high-density lipoprotein, tryglycerides), oxidative stress markers (GSH, SOD, Catalase) and inflammatory mediators (NFκB, IL-6, TNF-α) were measured. Brain, kidney, pancreas, liver was isolated for histopathological examinations.

### Results

Administration of NA and STZ increased BG level in rats at 72 hrs. These rats showed significantly more immobility time in FST on day 21 as compared to vehicle control rats indicating depression-like behaviour (57.50 ± 5.46 sec in control vs 213±5.28 sec in diabetic rats). Treatment with PTE (28 days) significantly mitigated the depression-like behaviour in SPT and OFT. PTE significantly improved IR and lipid profile and normalised the cortisol level, free radical scavengers and inflammatory mediators (Table 1). Morphological impairment of the pancreas, liver, kidney, brain in T2D rats were ameliorated by PTE.

### Conclusions

Pterostilbene, exhibited antidepressant activity in diabetic rats possibly by reducing IR, inflammatory mediators and ameliorating the HPA axis imbalance.

**TABLE 1** Behavioral and biochemical estimation of effect of PTE on Diabetes induced Depression like behaviour. CPCSEA approval (PCP/IAEC/PCL19)

| Sr. no | Parameters (n=6) | VC | STZ Control | MET(500) | FLX(10) | PTE(10) | PTE(20) | PTE(40) |
|---|---|---|---|---|---|---|---|---|
| 1. | OFT (Crossings) | 68.29±3.92 | 24.43±2.23$^{\#\#\#}$ | 34.00±3.16 | 67.14±6.32$^{***}$ | 38.00±2.04 | 44.29±3.92$^{**}$ | 47.62±5.25$^{***}$ |
| 2. | SPT | 76.55±3.25 | 33.65±3.20$^{\#\#\#}$ | 47.52±4.09 | 63.70±3.93$^{***}$ | 38.29±4.43 | 59.31±8.97$^{**}$ | 63.11±3.31$^{***}$ |
| 3. | %HOMA-IR | 292.1±33.98 | 710.9±34.47$^{\#\#\#}$ | 516.1±30.26$^{**}$ | 527.7±22.34$^{**}$ | 726.8±41.25 | 548.9±35.06$^{*}$ | 477.0±49.31$^{***}$ |
| 4. | Cholesterol (mg/dL) | 31.79±2.62 | 85.45±6.52$^{\#\#\#}$ | 39.94±5.32$^{***}$ | 86.47±2.96 | 72.36±8.45 | 57.98±6.20$^{**}$ | 45.10±4.34$^{***}$ |
| 5. | Triglyceride (mg/dL) | 87.28±5.830 | 159.6±10.92$^{\#\#\#}$ | 101.5±4.368$^{***}$ | 130.9±4.640 | 141.5±13.69 | 114.9±10.99$^{**}$ | 97.92±4.645$^{***}$ |
| 6. | HDL-C (mg/dL) | 56.88±2.22 | 22.61±1.34$^{\#\#\#}$ | 44.53±4.37$^{**}$ | 51.03±3.83$^{***}$ | 28.89±3.44 | 43.97±3.03$^{**}$ | 49.53±6.98$^{***}$ |
| 7. | LDL-C (mg/dL) | 33.17±2.712 | 103.3±6.11$^{\#\#\#}$ | 57.60±2.26$^{***}$ | 46.00±5.10$^{***}$ | 90.61±5.99 | 75.17±3.40$^{***}$ | 57.90±3.87$^{***}$ |
| 8. | SOD (ug/ml) | 1.79±0.13 | 0.54±0.06$^{\#\#}$ | 2.35±0.56$^{***}$ | 1.48±0.07$^{*}$ | 1.03±0.05 | 1.68±0.16$^{*}$ | 1.96±0.19$^{**}$ |
| 9. | GSH (ug/ml) | 58.00±4.87 | 27.17±3.03$^{\#}$ | 67.67±13.06$^{**}$ | 64.03±5.66$^{**}$ | 46.50±4.039 | 67.17±7.88$^{**}$ | 76.50±4.90$^{***}$ |
| 10. | Catalase (ug/ml) | 52.33±3.23 | 34.17±4.04$^{\#}$ | 55.50±6.42$^{**}$ | 52.00±3.41$^{*}$ | 35.50±3.17 | 50.50±4.81$^{*}$ | 58.00±2.54$^{**}$ |
| 11. | NF-κb (pg/ml) | 0.39±0.057 | 1.15±0.13$^{\#\#}$ | 0.49±0.12$^{*}$ | 0.50±0.13$^{*}$ | 1.28±0.26 | 0.56±0.10$^{*}$ | 0.52±0.12$^{*}$ |
| 12. | IL-6(pg/ml) | 136.4±19.92 | 881.0±39.58$^{\#\#\#}$ | 562.8±30.31+ | 563.2±23.85$^{**}$ | 633.8±65.81$^{*}$ | 445.0±93.94$^{**}$ | 193.3±30.15$^{***}$ |
| 13. | TNF-α (pg/ml) | 1.95±0.34 | 5.54±0.63$^{\#\#\#}$ | 3.58±0.53$^{*}$ | 3.68±0.40$^{*}$ | 5.52±0.22 | 3.75±0.55$^{*}$ | 2.95±0.32$^{*}$ |
| 14. | Cortisol (ug/ml) | 0.11±0.001 | 0.71±0.05$^{\#\#\#}$ | 0.48±0.065$^{*}$ | 0.46±0.03$^{*}$ | 0.65±0.06 | 0.48±0.04$^{*}$ | 0.48±0.057$^{*}$ |
| 15. | Body weight(g) | 250.4±2.442 | 227.8±2.442 | 235.4±2.952 | 240.0±2.847 | 231.6±3.438 | 239.9±2.199 | 242.3±2.717 |

The results were analyzed using Graph Pad Prism software (V8). Values are mentioned as mean ± SEM (n=6).
$^{\#}$P<0.05,
$^{\#\#}$P<0.01,
$^{\#\#\#}$P<0.001, vs Vehicle control;
*P<0.05,
**P<0.01,
***P<0.001 vs STZ-diabetic control.

### References

1. Mommersteeg PMC, et al. Diabet Med. 2013;30(6):208-215.
2. Oguntibeju OO. Int J Physiol Pathophysiol Pharmacol. 2019;11(3):45-63.

3. Estrela JM, et al. Crit Rev Clin Lab Sci. 2013;50(3):65-78.

## OC042 | Correlation of different serotonin 2A receptor signaling pathways of serotonergic psychedelics with reported human doses

**Deborah Rudin[1]; Dino Luethi[1]; Helene Rolli[1]; Marius Hoener[2]; Matthias Liechti[1]**
*[1]Division of Clinical Pharmacology & Toxicology, Department of Biomedicine and Department of Pharmaceutical Sciences, University Hospital Basel and University of Basel; [2]Neuroscience Research, pRED, Roche Innovation Center Basel, F. Hoffmann-La Roche Ltd.*

**Introduction**

With a prevalence of around 10%, depression and anxiety disorders are associated with significant health, social, and ecological impairment. Recent studies showed that psychedelics may be promising in the treatment of various neuropsychiatric and neurological disorders [1]. Interactions of psychedelics with the serotonin 2A receptor (5-HT2AR) predict their psychedelic properties and clinical potency. Since several 5-HT2AR signaling pathways as well as various techniques to assess the 5-HT2AR activation potency exists, we aimed to elucidate the most suited for the assessment of the clinical potency of psychedelics.

**Methods**

We investigated the activation of different signaling pathways of 23 different psychedelics at the 5-HT2AR and their correlation with reported human doses. As the 5-HT2AR is a G protein-coupled receptor, we focused on the dissociation of the different Gα subunits. We used transfected cells to assess the activation of the 5-HT2AR leading to phospholipase C (PLC) activation by measuring the accumulation of inositol monophosphate 1 (IP1) as well as calcium release. Additionally, we assessed the activation of the 5-HT2AR resulting in phospholipase A2 (PLA2) activation by facilitation of [3H]arachidonic acid release. Moreover, we assessed the binding affinity of the same psychedelics at the 5-HT2AR and correlated the binding affinity with reported human doses as well as with the activation potencies from the different signaling pathways.

**Results**

All investigated 5-HT2AR activation signaling pathways correlated well with reported human doses. IP1 accumulation displayed the highest correlation (Pearson R=0.9209; n=23) followed by PLA2 activation (Pearson R=0.8982; n=23) and calcium release showing the lowest correlation (Pearson R=0.8029; n=23). Binding affinities highly correlated with reported human doses (Pearson R=0.9710; n=23), as well as with activation potencies measured by IP1 formation (Pearson R=0.9266; n=23) and PLA2 activation (Pearson R=0.9192; n=23) and slightly less when measured by calcium release (Pearson R=0.8029; n=23).

**Conclusions**

To predict the psychedelic properties and clinical potency of serotonergic psychedelics, 5-HT2AR activation assessed by IP1 formation and PLA2 activation results in the most accurate prediction, highly correlating with human doses. Moreover, the binding affinity is highly predictive of the clinical potency of psychedelic 5-HT2AR agonists. However, unlike the activation potency, the binding affinity does not distinguish between agonists and antagonists. The development of novel effective treatment options for neuropsychiatric disorders will profit from optimized investigation tools to predict the psychedelic properties and clinical potency of known and novel psychedelics.

**Reference**

1. Nichols DE, Johnson MW, Nichols CD. Psychedelics as Medicines: An Emerging New Paradigm. Clin Pharmacol Ther. Feb 2017;101(2):209-219. https://doi.org/10.1002/cpt.557

## OC073 | P2X7 involves in the mouse retinal degeneration through the coordinate actions in different retinal cell types

**Ponarulselvam Sekar; Shu Lan-hsin; George Hsiao; Wan-Wan Lin; Chi-Ming Chan**
*Taipei Medical University*

**Introduction**

High concentrations of ATP released by dying cells are sensed as a danger signal by the P2X7 receptor. NaIO3 is an oxidative toxic agent and its retinal toxicity and degeneration have been used as the model of dry AMD.

**Methods**

In this study we used NaIO3-treated mice and cell models including BV-2 microglia, 661W photoreceptors, rMC1 Müller cells and ARPE-19 retinal epithelial cells to understand the pathological action of P2X7 in retinal diseases. We found that NaIO3 can significantly decrease the

photoreceptor function by reducing a-wave and b-wave amplitudes in ERG response. OCT analysis revealed the degeneration of retinal epithelium and ganglion cell layers.

**Results**

Interestingly, P2X7-/- mice were protected from the NaIO3-induced retinopathy and inflammatory NLRP3, IL-1β and IL-6 gene expression in retina. Hematoxylin and eosin staining indicated that the retinal epithelium was less deteriorated in the P2X7-/- mice compared to the WT group. Although P2X7 was barely detected in 661W, rMC1 and ARPE-19 cells, its gene and protein levels can be increased after NaIO3 treatment, leading to a synergistic cytotoxicity of BzATP and NaIO3 in ARPE-19 cells.

**Conclusions**

In conclusion, the paracrine action of ATP/P2X7 axis via cell-to-cell communication is important in NaIO3-induced retinal injury. P2X7 antagonist might be a potential therapy in inflammation-related retinal disorders.

## OC102 | Electrophysiological analysis of kappa opioid receptor activation in mouse paraventricular thalamus

**Eloise Kuijer[1]; Sarah Bailey[1]; David Heal[2]; Sharon Smith[3]; Sue Wonnacott[1]; Chris Bailey[1]**
*[1]University Of Bath; [2]DevelRx Ltd, University Of Bath; [3]DevelRx Ltd*

**Introduction**

Kappa opioid receptors (KOPrs) encode the dysphoric component of stress and are postulated to be involved in drug addiction. The paraventricular thalamus (PVT) integrates reward-related and stress-related information. Evidence for KOPrs in PVT in drug-seeking behaviour has emerged [1] although their precise role is unclear. Here, we investigate KOPr agonist-induced currents in PVT neurons: their distribution across the PVT, between ages and sexes, and co-expression with other GPCRs. KOPr effects on excitatory postsynaptic currents (EPSCs) were also determined.

**Methods**

Brain slices were from 15 male and 20 female C57BL/6J mice either 4- or 8-weeks-old. Whole-cell voltage-clamp recordings were performed on single PVT neurons [2] perfused with: KOPr agonist spiradoline (30 μM); KOPr antagonist norBNI (1 μM); mu opioid receptor (MOPr) agonist met-enkephalin (10 μM); MOPr antagonist CTAP [D-Phe-Cys-Tyr-D-Trp-Arg-Thr-Pen-Thr-NH2] (1 μM). Differences between sexes and ages were determined by unpaired t-tests. Anatomical locations were compared using one-way ANOVA. Co-expression of KOPr and MOPr was analysed using Chi-square test. EPSC effects were determined by paired t-test. Data shown as mean±SEM. Significance level: $p<.05$ (two-tailed).

**Results**

Pre- and postsynaptic recordings were made from 61 PVT neurons. In 50 postsynaptic recordings, 37 neurons responded to KOPr activation by inducing a GIRK-mediated current of 13.5±1.7pA. KOPr currents differed across the anterior-posterior axis with smaller currents in the medial PVT compared to more anterior regions (One-way ANOVA (location) $F(2,26)=3.7$, $p=0.039$) ($n=4$-13 per group). However, there were no differences found between sexes ($p=0.67$) ($n=13$-16 per group), nor ages ($p=0.63$) ($n=13$-16 per group). Interestingly, in 42 neurons tested for both KOPr and MOPr, 96% of KOPr+ neurons also expressed MOPr ($\chi2=45.1$, $df=3$, $p<0.0001$) and the KOPr response was smaller than the MOPr response (one-sample t-test against 100%: $t=9.2$, $df=27$, $p<0.0001$) ($n=29$). In 11 presynaptic recordings, KOPr activation did not affect EPSC frequency ($p=0.98$).

**Conclusions**

Despite the opposing functions in emotional valence where KOPr mediates aversion whilst MOPr reward, PVT neurons unexpectedly co-express both receptor subtypes. This work will aid understanding of KOPr in the PVT, a promising structure in maladaptive circuits.

**References**

1. Hartmann MC, Pleil KE (2021) Circuit and neuropeptide mechanisms of the paraventricular thalamus across stages of alcohol and drug use. Neuropharmacology 198:108748

2. Groom S et al (2020) A novel G protein-biased agonist at the mu opioid receptor induces substantial receptor desensitisation through G protein-coupled receptor kinase. Br J Pharmacol Epub ahead of print Nov 2020

## OC104 | Functional characterisation of a KCNB1 (Kv2.1) potassium channel variant (P17T) which causes developmental delay and speech apraxia but not seizures

**Emma Veale[1]; Alessia Golluscio[1]; Katheryn Grand[2]; John Graham[2]; Alistair Mathie[1]**
[1]*University Of Kent;* [2]*David Geffen School of Medicine at UCLA*

**Introduction**

Numerous pathogenic variants in KCNB1, which encodes the voltage-gated potassium channel, Kv2.1, are linked to developmental and epileptic encephalopathies and associated with loss-of-function, -regulation, and -expression of the channel [1]. A novel de novo Kv2.1 channel variant (P17T) has been identified using whole-exome sequencing and is clinically associated with neurodevelopmental disorders but not seizures. In this study, we characterize the functional properties of this novel variant.

**Methods**

Characterisation of wild type (WT) and P17T human Kv2.1 channel currents was carried out using the whole-cell patch clamp technique on transiently transfected tsA201 cells using previously described methods [2]. Data are expressed as mean ± 95% Confidence Intervals (n = cells). Statistical analyses used unpaired t tests.

**Results**

Kv2.1-P17T channel current was 621 ± 154 pA/pF (n = 13) at +50 mV, which was significantly larger (P < 0.0001) than Kv2.1-WT (294 ± 73 pA/pF, n = 16). The P17T mutation also significantly (p < 0.0001) enhanced current through Kv2.1/Kv9.3 heteromeric channels from 95 ± 98 pA/pF (n = 8) to 473 ± 108 pA/pF (n = 6). The P17T mutation shifted the steady-state inactivation to the right for both Kv2.1 homomeric channels ($V_{50}$ from -32.5 ± 1.0 mV to -23.7 ± 4.0 mV) and Kv2.1/Kv9.3 heteromeric channels ($V_{50}$ from -60.4 ± 2.3 mV to -31.6 ± 6.1 mV). The Kv2.1 blocker, guanxitoxin-1E (10 nM) reduced Kv2.1-WT current from 199 ± 30 pA/pF (n = 12) to 122 ± 39 pA/pF (n = 6), (p < 0.05) but had no effect on Kv2.1-P17T current (348 ± 63 pA/pF, n = 10, compared to 334 ± 40 pA/pF, n = 7 in the toxin). However, guanxitoxin-1E was effective on both Kv2.1-WT and Kv2.1-P17T channels at 100 nM.

**Conclusions**

We have shown that Kv2.1-P17T channels have a gain-of-function, with altered steady-state inactivation and reduced sensitivity to guanxitoxin-1E. The lack of seizures seen in this patient contrasts with most other patients with different KCNB1 mutations [1]. This may be because other variants result in a loss-of-function of the encoded Kv2.1 potassium channel, rather than the gain-of-function described here for the P17T variant.

**References**

1. Bar C et al. (2018) Expanding the genetic and phenotypic relevance of KCNB1 variants in developmental and epileptic encephalopathies: 27 new patients and overview of the literature. Human Mutation 41:69-80.
2. Mathie A et al. (2021) Heterologous expression of Ion channels in mammalian cell lines. Methods Mol Biol 2188:51-65.

## OC110 | Angiotensin II receptor type 1 antagonism enhances the antiallodynic effect of morphine in a rodent model of neuropathic pain

**David Á. Karádi[1]; Anna R. Galambos[1]; Nariman Essmat[1]; Kornél Király[1]; Imre Vörös[1]; Edina Szűcs[2]; Zoltán V. Varga[1]; Mahmoud Al-Khrasani[1]**
[1]*Department of Pharmacology and Pharmacotherapy, Semmelweis University;* [2]*Biological Research Center, Institute of Biochemistry*

**Introduction**

Despite the large arsenal of analgesic medications, neuropathic pain (NP) management is not solved yet. The role of the renin-angiotensin system - RAS - in the somatosensory system and its function in alleviating NP among others, is emerging as an important area of pain research. We have recently reviewed the possible interactions between the RAS and opioid system [1]. Herein, to the best of our knowledge, we are the first to demonstrate the effect of a combination of angiotensin II receptor type 1 (AT1) inhibitors and opioids in NP.

**Methods**

Male Wistar rats (n=5-6/group) underwent partial sciatic nerve ligation to induce mononeuropathic pain. They received acute or chronic oral treatment with AT1 antagonists losartan or telmisartan alone or in combination with subcutaneous morphine. The antiallodynic effect was determined by dynamic plantar aesthesiometer. Next, animals were sacrificed, and spinal cord samples were taken and subjected to morphine-stimulated [35S]-GTPγS binding assays. Spinal cord, dorsal root ganglion (DRG), and brain tissue samples were obtained from naive rats and used

for RNA Scope® in-situ hybridization, to determine OPRM1, Agtr1a, Agtr2 mRNA presence. Statistical significance was determined using ANOVA followed by Tukey's post hoc test.

**Results**

Losartan or telmisartan showed significant acute antiallodynic effect in doses of 100 and 80 μmol/kg, respectively (P<0.05 vs vehicle). Animals treated for 10 days with the combination of telmisartan and morphine in sub-analgesic doses (20 and 10 μmol/kg, respectively) improved the pain threshold of the operated paw (P=0.0524 vs non-operated paw) and caused a leftward shift in the morphine concentration-response curve in the [35S]-GTPγS binding assay (Table 1). On the other hand, the combination of losartan and morphine in sub-analgesic doses failed to show similar antiallodynia. Colocalization of angiotensin and μ opioid receptor mRNAs were detected at sites of particular importance for pain transmission in the superficial spinal cord, the DRG and the periaqueductal grey.

**Conclusions**

AT1 antagonist telmisartan, but not losartan augments morphine analgesia in our rodent NP model. This effect of telmisartan is concordant with the observed leftward shift in the concentration-response curve of morphine in the spinal cord of animals treated with the combination of telmisartan and morphine. These data can be interpreted as favourable changes in spinal plasticity for analgesia.

**TABLE 1** Morphine-stimulated [$^{35}$S]-GTPγS binding data on spinal cords obtained from animals undergoing 10 days of chronic treatment

| | GTPγS binding | |
|---|---|---|
| **Treatment group (10 days of treatment)** | **EC50 ± S.E.M. (nM)** | **Emax ± S.E.M. (%)** |
| vehicle + saline (n=5) | 205.8 ± 120.6 | 134.9 ± 3.6 |
| vehicle + morphine (n=5) | 1190.0 ± 607.5*$^{\delta}$ | 138.7 ± 4.4 |
| telmisartan + morphine (n=5) | 153.1 ± 75.6 | 135.3 ± 2.7 |

*P<0.05 vs telmisartan + morphine; $^{\delta}$P<0.05 vs vehicle (1% hydroxyethyl cellulose) + saline

**Reference**

1. K. Király et al., "Shedding light on the pharmacological interactions between μ-opioid analgesics and angiotensin receptor modulators: A new option for treating chronic pain," Molecules, vol. 26, no. 20. 2021. https://doi.org/10.3390/molecules26206168

## OC117 | Cannabidiol interacts TRPA1 channel to promote analgesic effects: docking insights

**Joelmir Lucena Veiga da Silva[1]; Gisele Evelin de Jesus Arruda[1]; Nathalia Napoli Mendes[1]; Gidelson José Silva Júnior[1]; Gustavo Napoli Mendes[1]; Neuton Barbosa Dantas Lira[1]; Ana Carolina Oliveira Aguiar[1]; Cintia Yoko Morioka[2,3]; Alessandra Ermetice de Almeida Costa[4]**

*[1]School of Medicine of Olinda; [2]Advantage Health; [3]University of Sao Paulo; [4]Federal University of Sao Paulo*

**Introduction**

Transient receptor potential channel subfamily A member 1 (TRPA1) is a $Ca^{2}$+-permeable cation channel that serves as one of the primary sensors of environmental irritants and noxious substances. TRPA1 is associated with inflammatory pain and acute and chronic itch syndromes. Thus, it is a therapeutic target for the treatment of these types of diseases. So far, TRPA1 have been involved in the therapeutic action of cannabidiol (CBD) regarding the management of pain. Patch clamp analysis demonstrated that CBD activated and rapidly desensitized TRPA1 and CBD also stimulated and desensitized human TRPA1 using calcium assays and enzymatic assays [1,2]. Although CBD is known to activate and desensitize TRPA1, there have not been docking studies that present CBD binding sites on TRPA1. Therefore, our aim was to analyze the interactions of CBD on TRPA1.

**Methods**

A quantitative and experimental research with an in silico approach that used the CBD (CID 644019) and 2-chloro-N-[4-(4-methoxyphenyl)-1,-3-thiazol-2-yl]-N-(3-methoxypropyl)acetamide (JT010, CID 18524489), an agonist TRPA1, from PubChem was performed. For docking studies, the Cryo-EM structure of the human TRPA1 ion channel was retrieved from Protein Data Bank (ID 6PQO). The output conformers from Dockthor®, a receptor-ligand docking program, were ranked in order of increasing affinity with the protein. The standard evaluations were 1,000.000 using blind docking and 884,736 grid points. The affinity predictions (Aff) were obtained and compared using Student t-test, where values p<0.05 were significant.

**Results**

There were three conformers that showed greater binding affinity into CBD (Aff=-7.19±0.03 kcal/mol) and JT010 (Aff=-7.86±0.05 kcal/mol) with the TRPA1. The comparing Aff of CBD and JT010 revealed a significant difference (p=0.0002), showing that agonist TRPA1 had most affinity than CBD. The CBD interacted with 514, 516 and 517 resides. The JT010 thiazol group formed CH-π interaction with 186 reside, the methoxyphenyl group interacted with 146, 249, 579 and 582 resides. Thus, the data showed that CBD and JT010 present distinct sites of binding on TRPA1.

**Conclusions**

Our structural and docking studies reinforce the analgesic effects of cannabidiol that bind and desensitize TRPA1.

**References**

1. De Petrocellis L, Ligresti A, Moriello AS et al. Effects of cannabinoids and cannabinoid-enriched Cannabis extracts on TRP channels and endocannabinoid metabolic enzymes. Br J Pharmacol.2011;163;1479–1494.

2. Iannotti FA, Hill CL, Leo A, et al. Nonpsychotropic plant cannabinoids, cannabidivarin and cannabidiol, activate and desensitize transient receptor potential vanilloid 1 channels in vitro: potential for the treatment of neuronal hyperexcitability. ACS Chem Neurosci.2014;5:1131-1141.

## OC131 | Contribution of disrupted gastrointestinal myoelectrical activity to mechanisms of cisplatin-induced acute and delayed nausea and emesis

**Aleena Khalid; Zengbing Lu; Man-piu Ngan; John Anthony RUDD**
*School of Biomedical Sciences, Faculty of Medicine, The Chinese University of Hong Kong*

**Introduction**

Current anti-emetic guidelines for the treatment of chemotherapy-induced emesis include the use of 5-HT3 and NK1 receptor antagonists in combination with a glucocorticoid. Unfortunately, ~20% of patients remain unprotected. In this study, we evaluate whether the 5-HT3 receptor antagonist, palonosetron, NK1 receptor antagonist, netupitant, and the glucocorticoid, dexamethasone, prevents emesis and cisplatin-induced disruption of gastric myoelectric activity (GMA) in ferrets.

**Methods**

Ferrets were surgically implanted with radio-telemetric transmitters to record GMA, blood pressure (BP) and core body temperature (CBT); behaviour was also recorded; forming a set of physiological changes indicative of nausea (PCIN). 24 h baseline recordings were obtained prior to the administration of palonosetron (1 mg/kg, p.o, in dH2O, n=7), netupitant (3 mg/kg, p.o, in 0.3% tween 80, n=8) or dexamethasone (1 mg/kg, i.p, three times/day, in saline, n=8) followed by cisplatin (5 mg/kg, i.p.). Recordings proceeded for a further 72 h.

**Results**

Cisplatin induced acute and delayed emetic response and decreased bodyweight, food and water intake. During the acute phase, slow wave dominant frequency (DF) remained unchanged but dominant power (DP) decreased significantly. An associated increase in delayed phase % normogastria and decrease in % tachygastria occurred (Table 1). Cisplatin increased BP and heart rate (HR); heart rate variability (HRV) decreased. Palonosetron protected 7/7 ferrets from acute emesis but failed to reverse cisplatin-induced decrease in bodyweight, food and water intake. Palonosetron increased DF (both phases) but BP was unaffected; a decrease of delayed phase HR occurred (Table 1). Netupitant significantly antagonised cisplatin-induced emetic response but had no effect on bodyweight, food and water intake. Netupitant increased acute phase % tachygastria and increased delayed phase DF. Netupitant reduced cisplatin-induced increases in BP, HR and reversed changes in HRV during the delayed phase. Dexamethasone antagonised cisplatin-induced delayed emetic response and increased water intake. In both phases, % normogastria decreased while % bradygastria increased but DF and DP only increased during the delayed phase (Table 1). Significant increases in BP (delayed phase) and HRV (both phases), while reductions in HR (both phases) and CBT (acute phase) occurred (Table 2).

**Conclusions**

All three treatments had predictable effects to antagonise emesis. However, palonosetron antagonised cisplatin-induced disruptions in acute phase DF whereas netupitant antagonised DF, BP, HR, and HRV during the delayed phase. Dexamethasone increased DF and DP in the delayed phase but affected cardiovascular control. We propose that the GMA data may have relevance to mechanisms involved in both 'nausea' and emesis.

**TABLE 1** Data represents mean ± SEM. Significant differences relative to cisplatin shown as *p < 0.05, **p<0.01, ***p<0.001 and relative to vehicle shown as $^{\#}$p < 0.05, $^{\#\#}$p<0.01, $^{\#\#\#}$p<0.001 (Two-way ANOVA, followed by Šidák test)

| DF (% change) | | | | | |
|---|---|---|---|---|---|
| | **Vehicle** | **Cisplatin** | **Palonosetron** | **Netupitant** | **Dexamethasone** |
| **0-24h** | -0.36 ± 1.35 | -1.94 ± 0.64 | 6.05 ± 1.52* | 4.56 ± 1.49 | 0.11 ± 1.52 |
| **24-48h** | 0.10 ± 1.41 | -1.66 ± 2.30 | 6.67 ± 2.14* | 6.11 ± 0.83* | 3.28 ± 1.92 |
| **48-72h** | 0.34 ± 1.45 | -4.20 ± 5.14 | 7.90 ± 2.47*** | 8.64 ± 0.87*** | 6.74 ± 1.55*** |
| **DP (% change)** | | | | | |
| | **Vehicle** | **Cisplatin** | **Palonosetron** | **Netupitant** | **Dexamethasone** |
| **0-24h** | 5.19 ± 14.8 | -49.20 ± 10.20$^{\#}$ | -28.06 ± 4.34 | -52.85 ± 6.86 | -62.80 ± 4.23 |
| **24-48h** | -13.65 ± 17.25 | -54.47 ± 12.29 | -54.02 ± 10.3 | -69.48 ± 7.68 | -51.78 ± 12.09 |
| **48-72h** | -1.88 ± 17.14 | -49.34 ± 18.21$^{\#}$ | -66.19 ± 6.64 | -73.30 ± 3.99 | -2.07 ± 28.98* |
| **% Power Bradygastria (% change)** | | | | | |
| | **Vehicle** | **Cisplatin** | **Palonosetron** | **Netupitant** | **Dexamethasone** |
| **0-24h** | 16.00 ± 19.05 | 31.43 ± 10.10 | 10.16 ± 12.42 | 23.03 ± 21.26 | 98.89 ± 24.03* |
| **24-48h** | 34.23 ± 29.09 | -13.94 ± 12.17 | -17.81 ± 8.70 | 7.22 ± 19.64 | 88.37 ± 21.57*** |
| **48-72h** | 4.75 ± 12.91 | -23.36 ± 6.98 | -22.00 ± 10.65 | -5.82 ± 20.88 | 61.69 ± 24.69** |
| **% Power Normogastria (% change)** | | | | | |
| | **Vehicle** | **Cisplatin** | **Palonosetron** | **Netupitant** | **Dexamethasone** |
| **0-24h** | -4.73 ± 4.94 | -1.49 ± 8.05 | 4.29 ± 3.34 | -4.60 ± 9.42 | -29.66 ± 5.57* |
| **24-48h** | -6.24 ± 6.44 | 24.50 ± 10.54$^{\#\#}$ | 16.97 ± 3.08 | 23.15 ± 9.41 | -17.38 ± 6.28*** |
| **48-72h** | -3.09 ± 5.48 | 26.05 ± 9.08$^{\#}$ | 18.72 ± 5.99 | 30.40 ± 7.19 | -1.81 ± 8.51* |
| **%Power Tachygastria (% change)** | | | | | |
| | **Vehicle** | **Cisplatin** | **Palonosetron** | **Netupitant** | **Dexamethasone** |
| **0-24h** | 20.86 ± 13.72 | -37.21 ± 9.79$^{\#}$ | -24.77 ± 8.09 | 35.93 ± 36.01*** | 10.16 ± 15.23 |
| **24-48h** | 12.90 ± 18.32 | -55.66 ± 6.39$^{\#\#}$ | -43.16 ± 9.99 | -44.63 ± 5.96 | -19.69 ± 9.01 |
| **48-72h** | 24.14 ± 17.14 | -47.62 ± 12.18$^{\#\#\#}$ | -52.01 ± 7.89 | -57.96 ± 6.71 | -33.25 ± 11.78 |

**TABLE 2** Data represents mean ± SEM for episodes of emesis while median ± IQR for latency. Significant differences relative to cisplatin shown as **p < 0.01 and ***p<0.001 (One-way ANOVA, followed by Bonferroni test)

| | **Drug groups** | | | |
|---|---|---|---|---|
| **Episodes of emesis** | **Cisplatin** | **Palonosetron** | **Netupitant** | **Dexamethasone** |
| **0-24h** | 17.5 ± 9.4 | 0.7 ± 0.7 | 0.6 ± 0.3 | 1.5 ± 1.4 |
| **24-72h** | 34.0 ± 4.4 | 37.6 ± 8.8 | 7.3 ± 2.8** | 1.5 ± 1.1*** |
| **Latency (h)** | 3.2 (1.2-21.4) | 30.2 (29.1-35.6) | 14.9 (5.1-89.8) | 79.4(18.4-96.0)** |

# OC132 | HIV-1 gp120-derived amyloid peptides as pathogenic factors promoting the progression of HIV-associated neurocognitive disorders

**Shuwen Liu; Chan Yang**
*Southern Medical University*

**Introduction**

The envelope protein gp120 of HIV have been proposed as contributing factors to HIV-associated neurocognitive disorder (HAND). Our previously study showed the β-strand in gp120 could formed amyloid fibrils by self-assembly and enhanced HIV-1 infection [1]. We herein found that amyloid peptides derived from gp120 in the brain tissue, which induced the occurrence and development of HAND.

**Methods**

HIV-1 gp120 transgenic (Tg-gp120) mice and HAND patients were selected to evaluate gp120-induced neuropathy based on histopathological and behavioral methods. The presence of gp120-derived amyloid fibers was identified by Congo red/Thioflavin T (ThT) staining combined with immunohistochemistry and immunofluorescence. The morphology of amyloid fibers in brain tissue and cerebrospinal fluid (CSF) of HAND patients and Tg-gp120 mice was observed by transmission electron microscopy (TEM). The sequence of GP120-derived amyloid peptides (GAPs) was identified by peptidomes combined with LC-MS/MS. The secondary structure of the GAPs was detected by Circular dichroism.

**Results**

Firstly, the neurotoxicity and neuropathy induced by gp120 were confirmed in vivo (Fig.1). Then, the amyloid fibrils was identified in the brain tissue of Tg-gp120 mice, which could be recognized by gp120 antibody, and was mainly located in the cortex and hippocampus (CA1, CA3 and DG) regions (Fig.2). Micromorphology of the amyloid fibrils in the brain tissue and CSF of Tg-gp120 mice was further verified by TEM (Fig.3). Corresponding to that, amyloid fibrils were detected in the CSF of HAND patients (Fig.4). Meanwhile, GAPs, including GP-3-6 and GP-14/GP-18, were identified by LC-MS/MS in brain tissue of Tg-gp120 mice and the CSF of HAND patients, respectively (Fig.5, Fig.6). Further mechanistic studies suggest that the C-C Chemokine Receptors 5 (CCR5) participates in the CNS damage induced by gp120 and GAPs (Fig.7). Maraviroc, a small molecule CCR5 antagonist, has been shown to improve the neuropathological injury and enhance the spatial learning and memory ability of Tg-gp120 mice (Fig.8).

**Conclusion**

This study for the first to identify GP120-derived amyloid peptides in brain tissue, which may be involved in HAND progression by activating the neuron CCR5. GAPs points out diagnostic agents for HAND and Maraviroc, an FDA-approved HIV entry inhibitor, is expected to provide clinical therapeutics for HAND.

# HIV-1 gp120-derived amyloid peptides as pathogenic factors promoting the progression of HIV-associated neurocognitive disorders

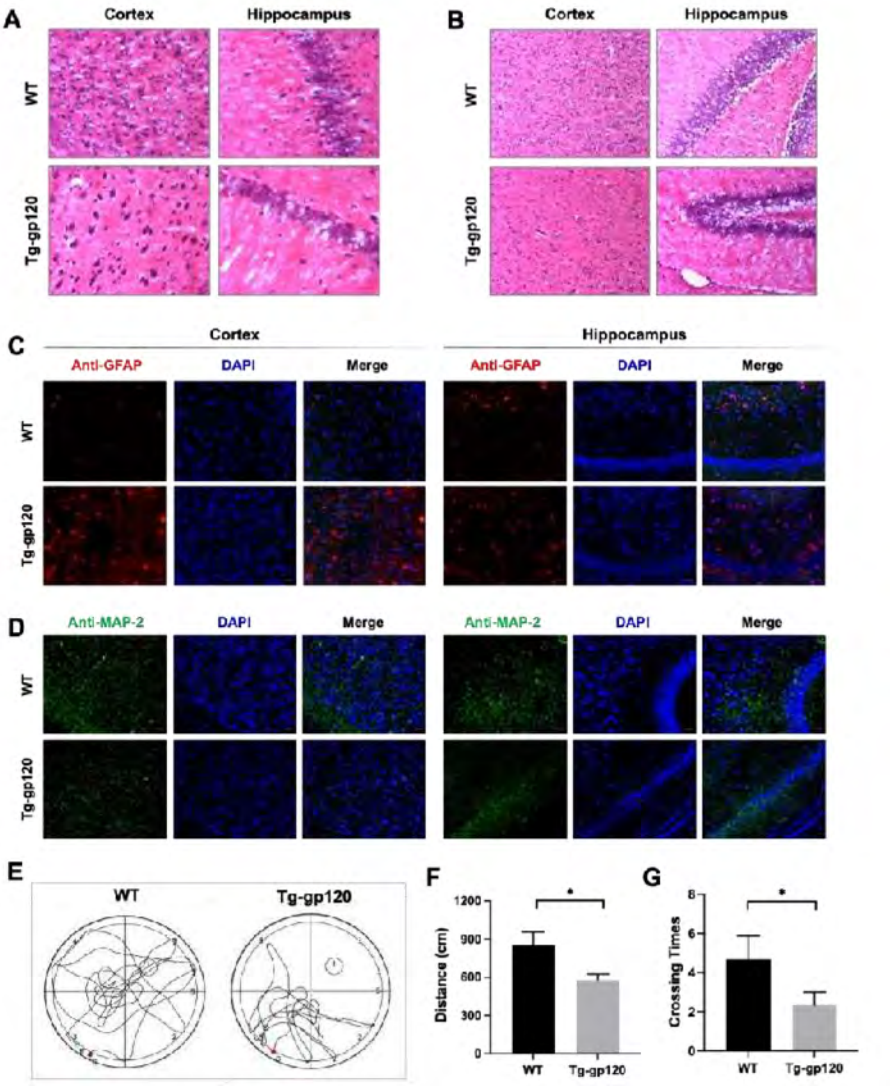


**Figure.1 HIV-1 gp120 Induced Neurotoxicity and Cognitive Impairment. A-B:** The pathological morphology of mouse brain tissue were observed by HE staining, Scale bar, 50 μm. **C-D.** Brain sections of the cortex and hippocampus were immunostained with GFAP **(C)** and MAP-2 **(D)**, scale bar, 20 μm. **E-G.** Total travel distance **(F)**, annulus crossings **(G)** of mice were analysis during the Morris water maze tests **(E)**.

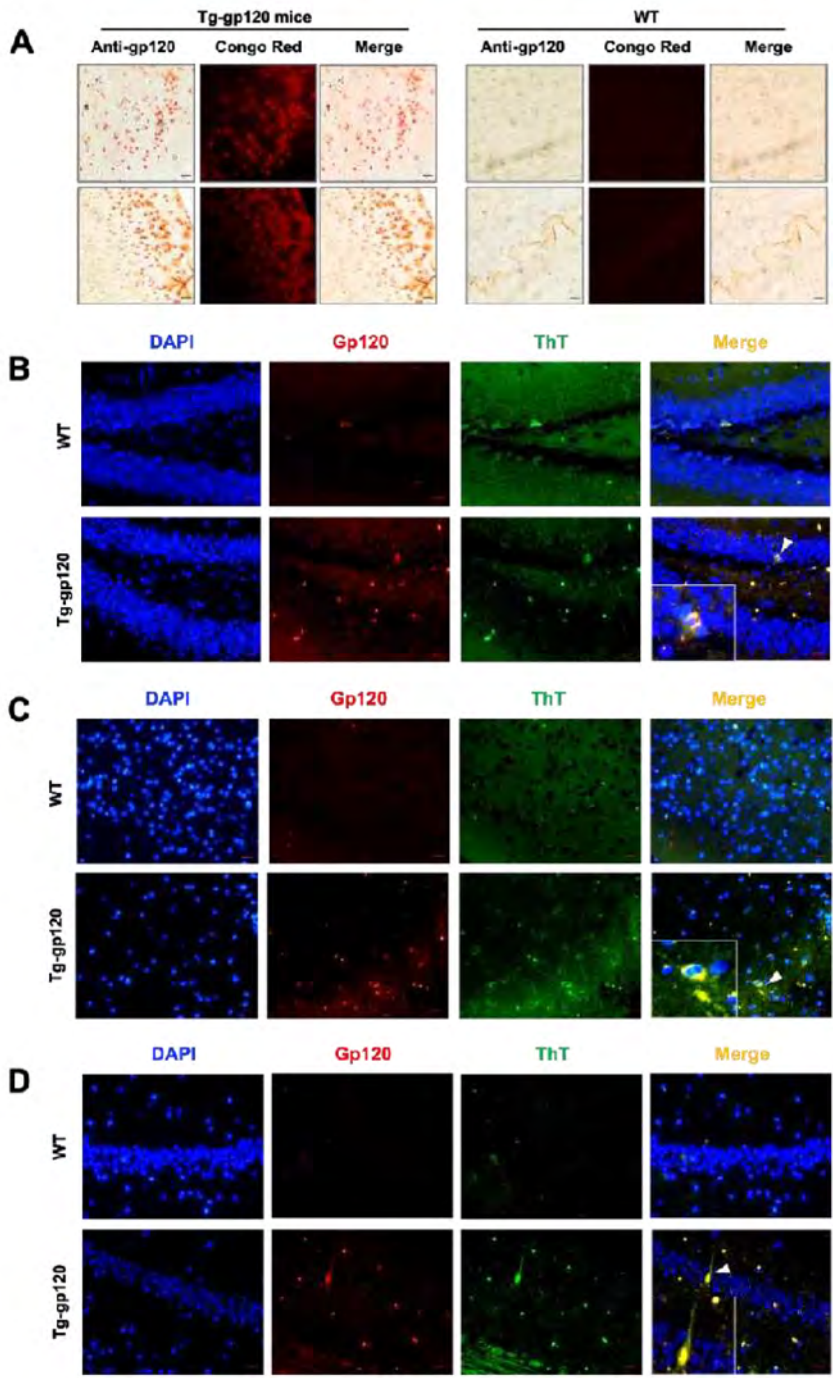


**Figure.2 Identification of gp120-derived amyloid fibers in the cortex and hippocampus of Tg-gp120 mice. A:** Mice brain were double labeling with gp120 (IHC) and Congo Red staining, Scale bar, 20 μm. **B-D:** Double staining were conducted on the brain amyloids using anti-gp120 (red) and ThT staining (green), Scale bar, 20 μm.

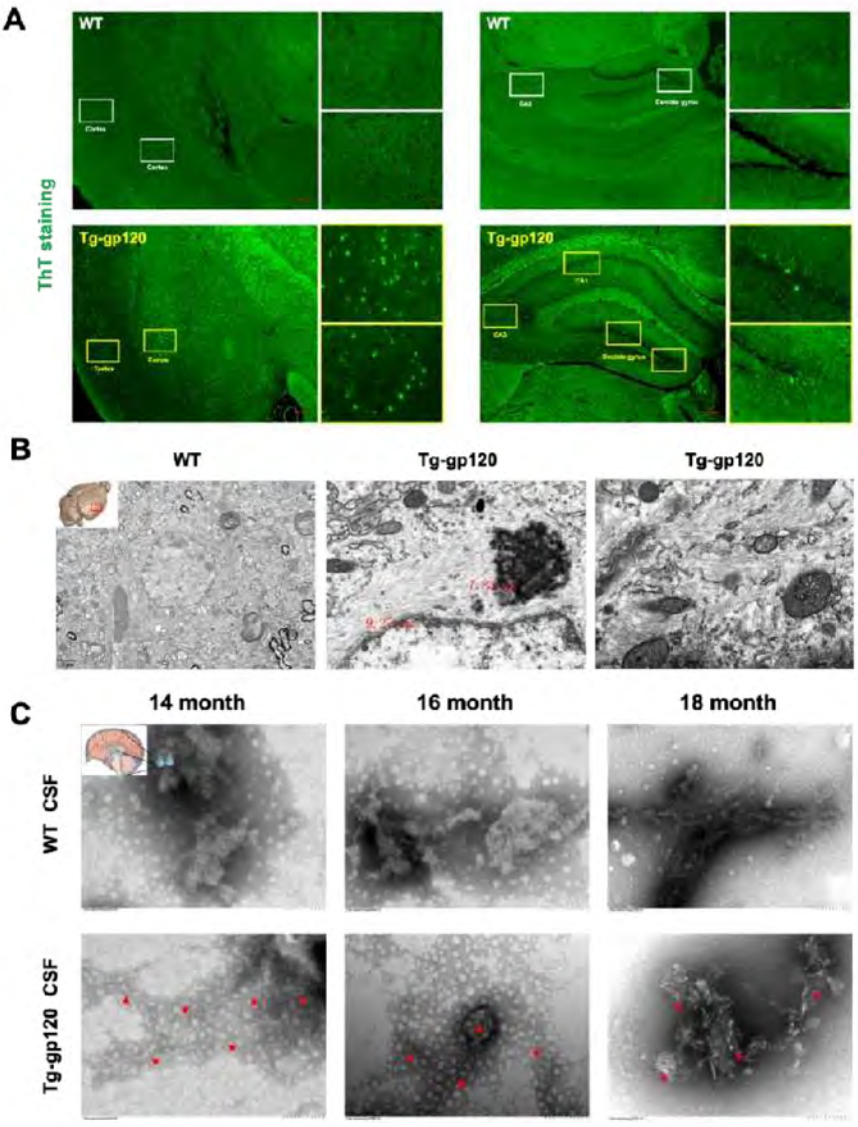


**Figure.3 Detection of amyloid fibrils in brain tissue of Tg-gp120 mice. A:** ThT staining (green) was used to detected the amyloid fibrils in cortex and hippocampus (CA1, CA3 and DG) of 14 month mice, scar bar: 50 μm; **B:** TEM micrographs of cortex, scar bar: 200 nm. **C:** TEM micrographs of CSF from mice, scar bar: 100 nm.

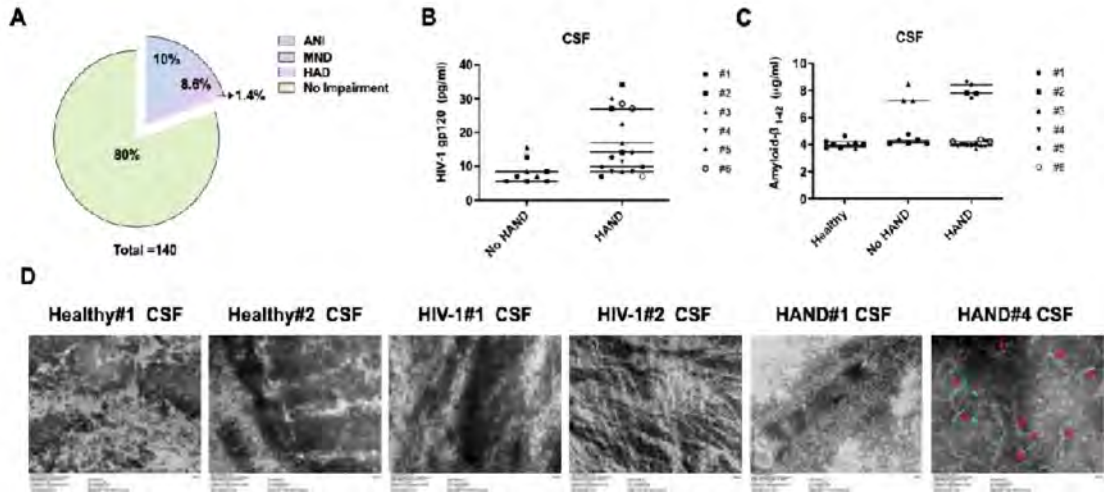


**Figure.4 Detection of amyloid fibrils in CSF of HAND patient. A:** Incidence of HAND and its subtypes (You 'an Hospital, China). **B-C:** The levels of gp120 and $A\beta_{1\text{-}42}$ in CSF of HAND patients were determined by ELISA. **D:** TEM micrographs of CSF extracted from the of normals, HIV infections and HAND patients, respectively.

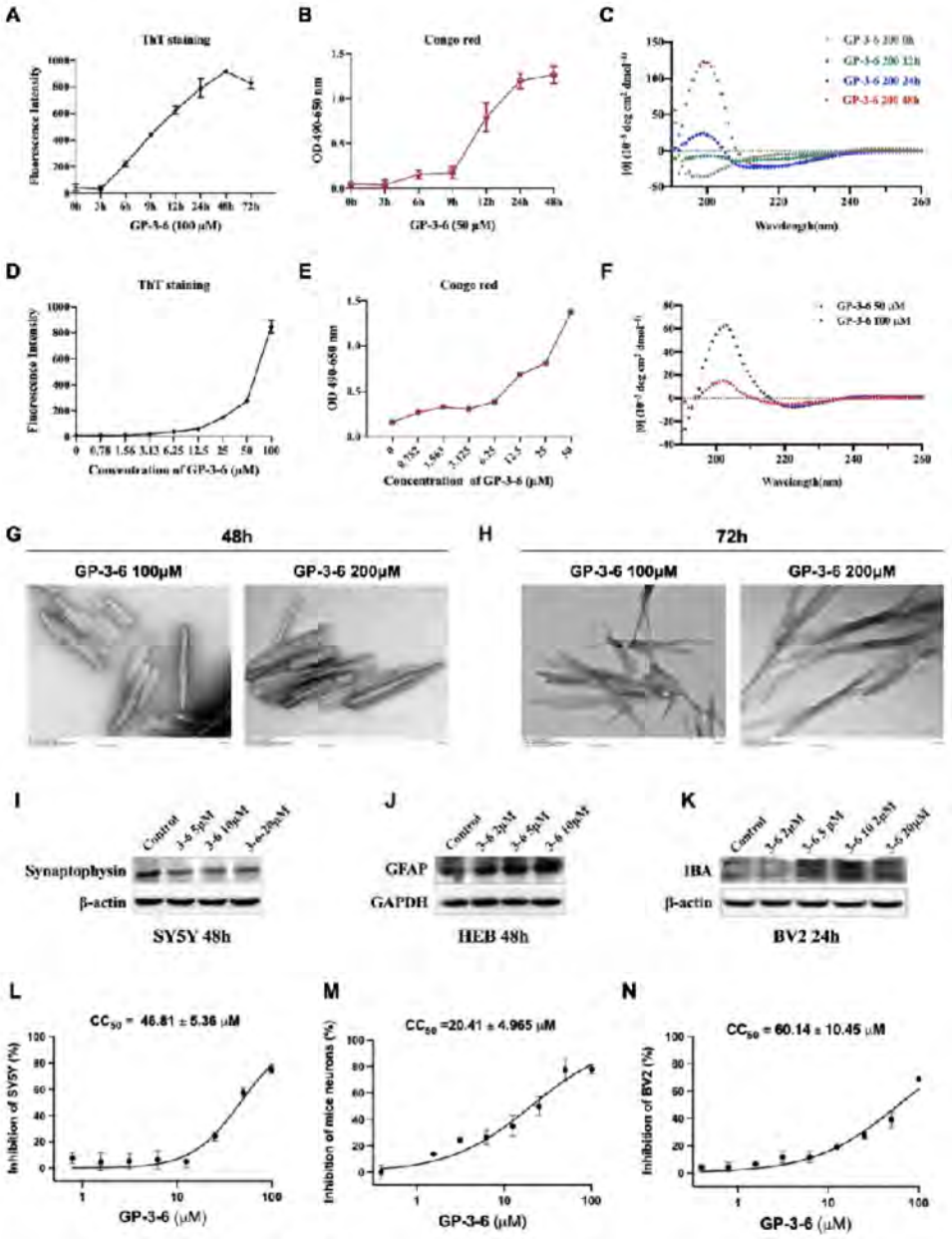


**Figure.5** The amyloid fiber formation process and secondary structure of GP-3-6 from mouse brain tissue were detected by ThT staining **(A, D)**, Congo red staining **(B, E)**, CD **(C, F)** and TEM **(G, H)**, and the neurotoxicity was verified *in vitro* **(I-N)**.

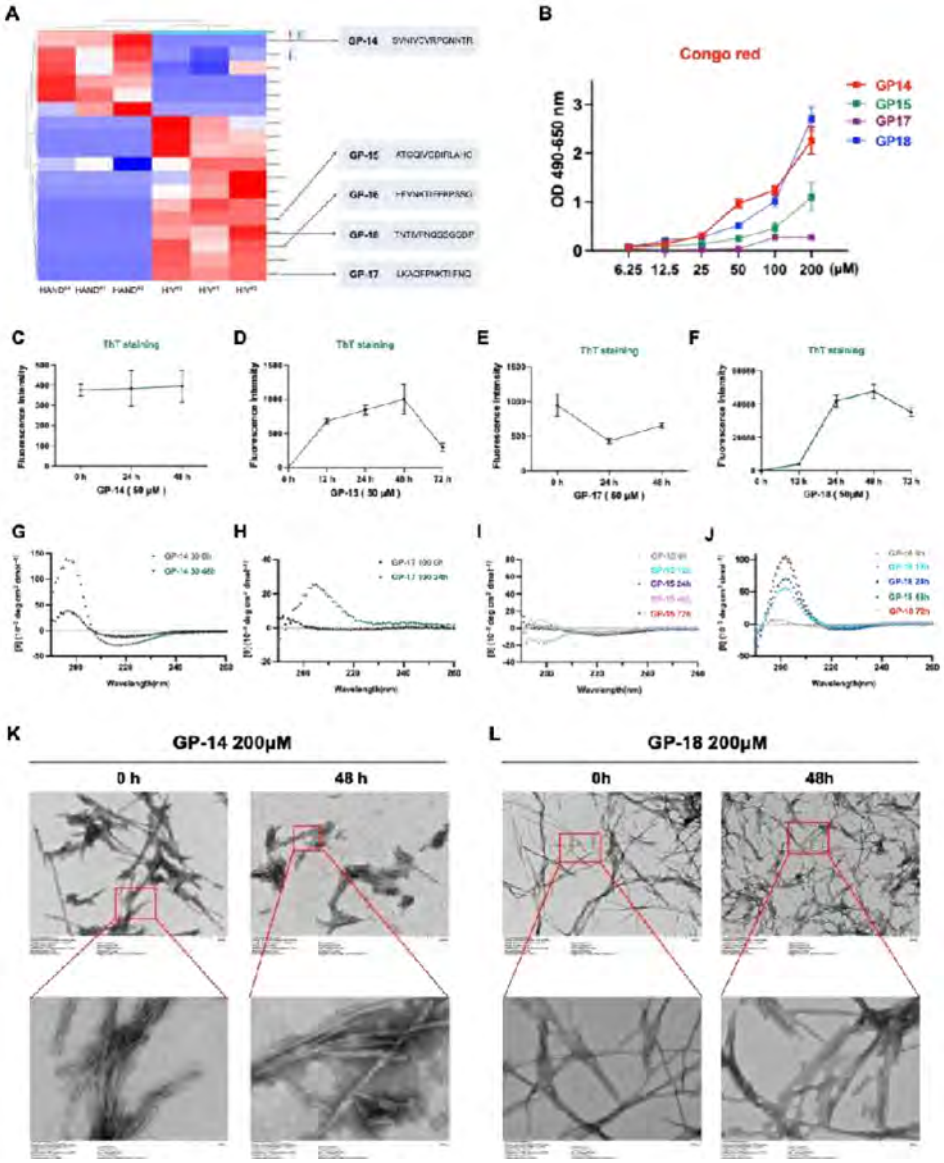


**Figure.6 Identification of GAPs from HAND patients. A:** GAPs in CSF of HAND patients identified by peptiomics combined with LC-MS/MS. **B-J:** Congo red staining **(B)**, ThT staining **(C-F)**, CD **(G-J)** and TEM **(K, L)** were used to characterize amyloid fiber and secondary structure.

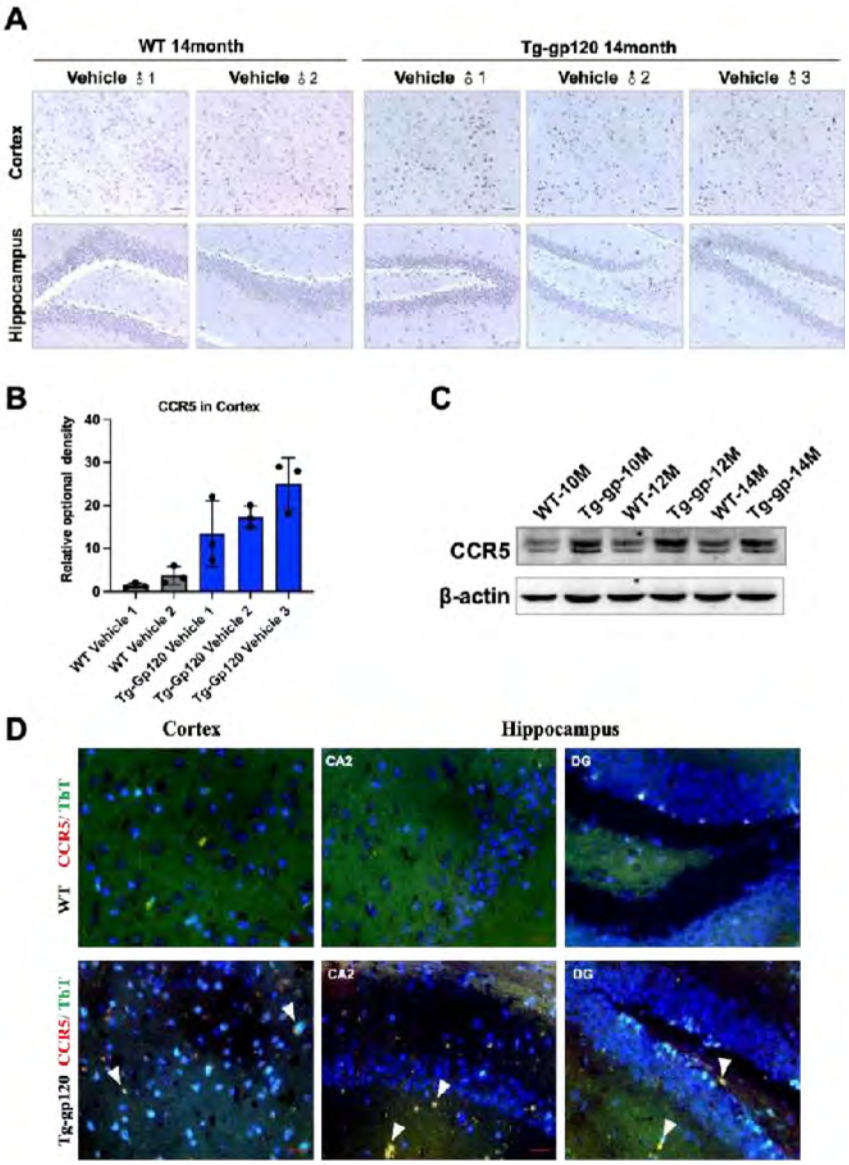


**Figure.7 CCR5 is involved in neurotoxicity induced by gp120 and GAPs.** The upregulation of CCR5 in brain tissue of Tg-gp120 mice was detected by IHC **(A-B)** and Western blot **(C). D:** Co-staining of anti-CCR5 (red) and amyloids (green) in cortex and hippocampus of Tg-gp120 mice, scar bar, 20 μm.

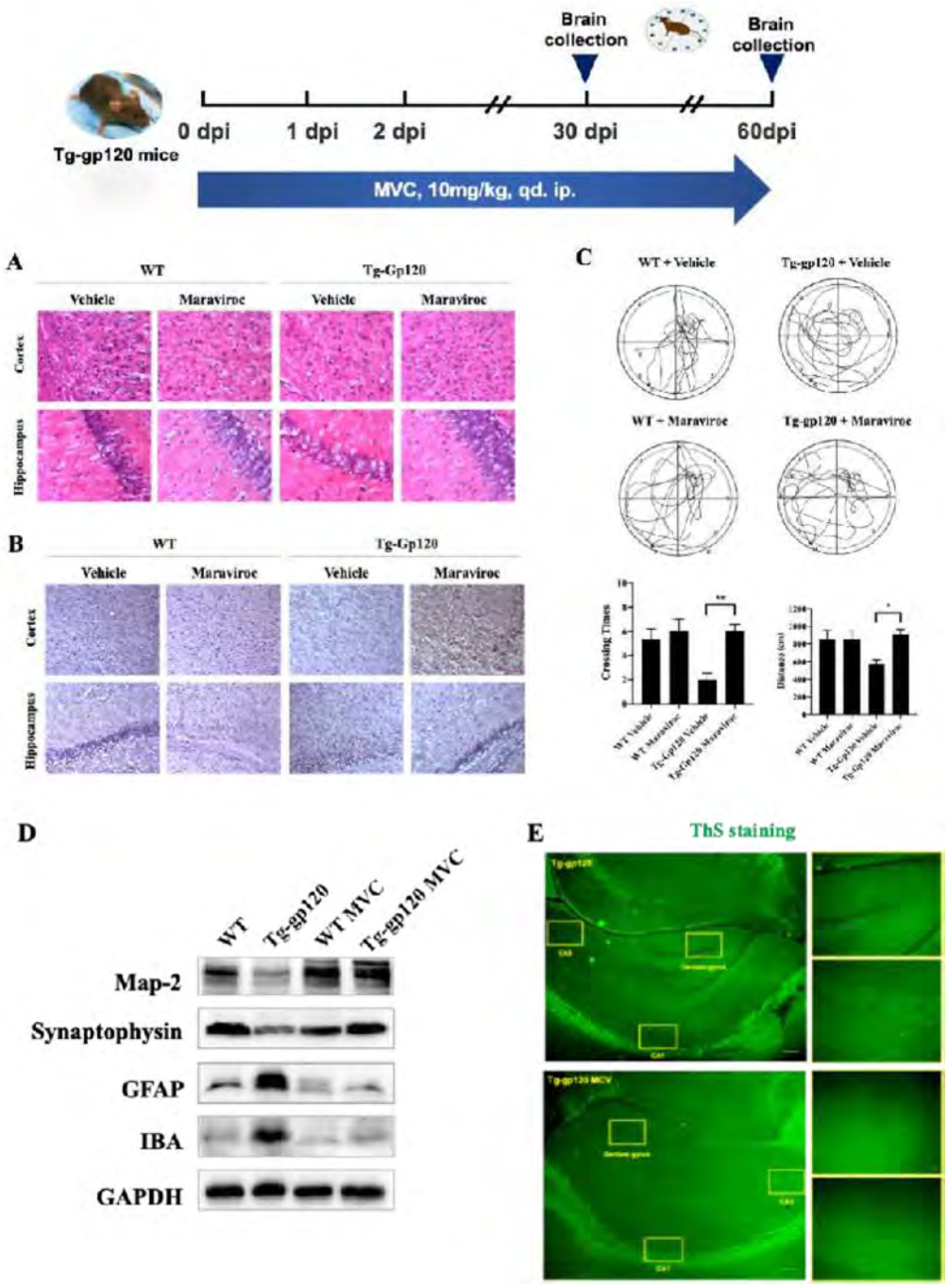


**Figure.8** Maraviroc (MVC) improved the neuropathological injury and enhanced the spatial learning and memory ability of Tg-gp120 mice.

**Reference**

1. Tan S, Li L, Lu L, et al. Peptides derived from HIV-1 gp120 co-receptor binding domain form amyloid fibrils and enhance HIV-1 infection. FEBS Lett. 2014; 588:1515-1522.

# OC133 | Divergent projections of the prelimbic cortex mediate autism- and anxiety-like behaviors

**Yi-Fan Luo**
*Nanjing Medical University*

**Introduction**

Autism spectrum disorder (ASD) is an intractable neuropsychiatric disorder while anxiety disorder is the most common psychiatric disorder in the world. There is increasing evidence that ASD and anxiety are highly comorbid conditions, and understanding the mechanisms of comorbidity is essential for therapeutic strategies for ASD. However, the underlying pathological mechanism of the comorbidity remains unclear. It is of great significance to take into account both molecular signal and circuit regulation for elucidating the pathological mechanism of autism-anxiety comorbidity.

**Methods**

In this study, we employed a multi-disciplinary approach combining bioinformatic analysis, behavioral tests, immunohistochemistry, patch clamp recordings, in vivo electrophysiological recordings, optogenetics, chemogenetics and gene regulation. Investigators were blinded to the groups and samples during the experiments for where applicable. The variance between the groups is similar. Data analyzed by unpaired t test were pre-tested for equal variance by F-test. For two normally distributed groups, significances were calculated by unpaired two-tailed Student's t-test. One-way ANOVA followed by Tukey's post hoc test or two-way ANOVA followed by Sidak's post hoc test were used for multiple-group comparisons. Kolmogorov-Smirnov test was used to compare M/L distribution of the 2 subpopulations of neurons in PL. All values represented using mean ± SEM. Significant differences are indicated when P value < 0.05 (*P < 0.05, **P < 0.01, ***P < 0.001).

**Results**

Tmem74 deficient in prelimbic cortex (PL) of mice results in anxiety-like and autistic-like behaviors, together with hyperexcitability of pyramidal neurons in PL. Two anatomically distinct subpopulations of PL pyramidal neurons project to the dSTR and BLA, mediating autistic-like and anxiety-like behaviors respectively. Reintroduction of TMEM74 into PL via AAV vector reduced the excitability of PNs in PL of Tmem74-/- mice, which could alleviate autistic-like and anxiety-like behaviors.

**Conclusions**

In conclusion, our study reported a new rodent model of autism-anxiety comorbidity and explored the pathogenesis of autism-anxiety comorbidity from the perspective of molecule and circuit, which might shed light on the treatment of comorbidity via targeting TMEM74 signaling in PL-related circuits.

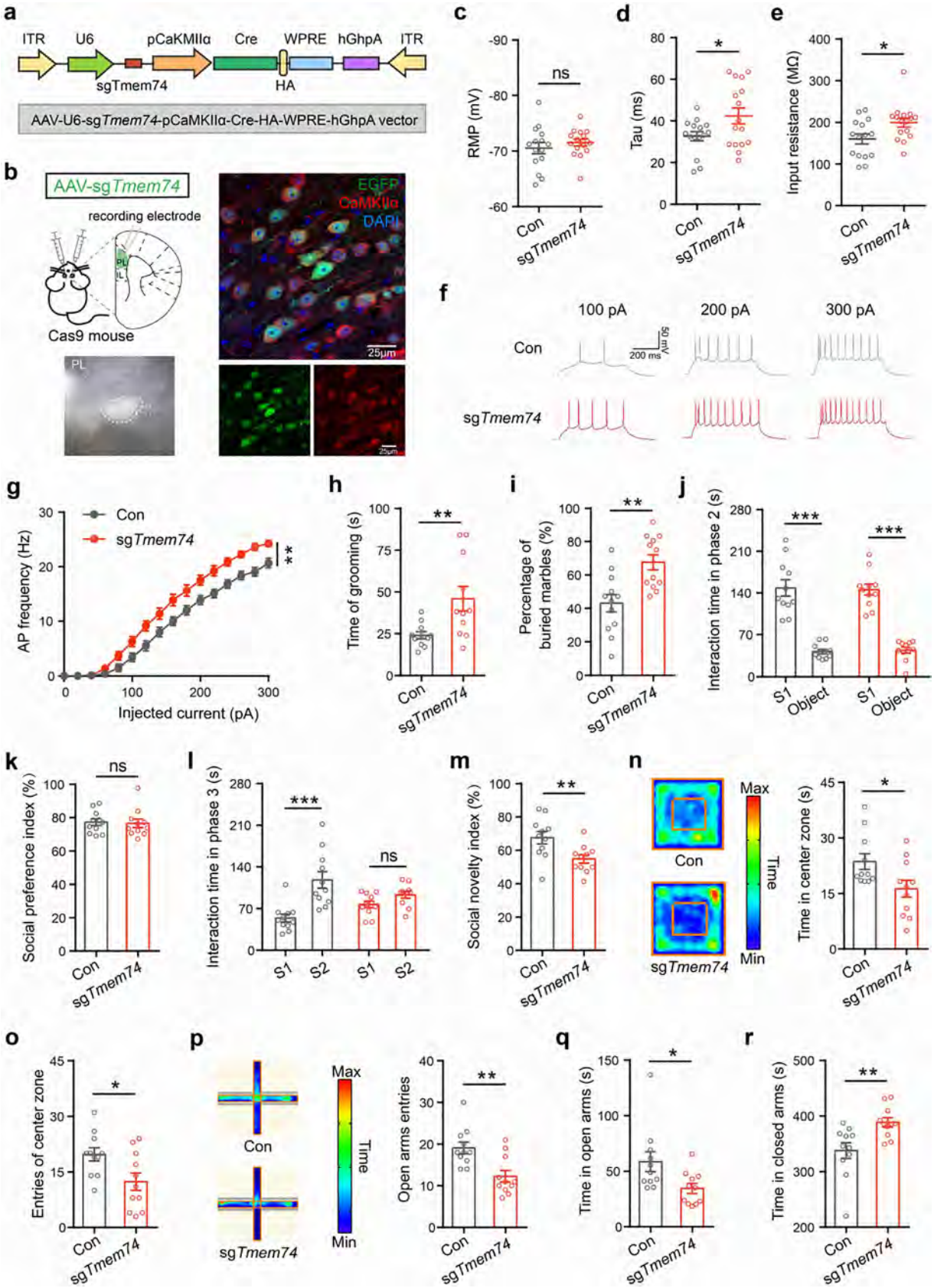

**Fig. 1 Selective deletion of *TMEM74* in PL leads to autism- and anxiety-like behaviors. c-e,** Membrane properties of pyramidal neurons in PL of control (Con) or AAV-sg*Tmem74*-injected mice (sg*Tmem74*), RMP (**c**), Tau (**d**) and Rin (**e**) (n=15 cells from 4 control mice, n=16 cells from 3 AAV-sg*Tmem74*-injected mice). **g** Quantification of AP frequency by current injections from 0 to 300 pA (stepped by 20 pA) (n=15 cells from 4 control mice, n=16 cells from 3 AAV-sg*Tmem74*-injected mice). **h, i** The time spent on grooming (**h**) and the percentage of buried marbles (**i**) in mice in selectively loss of *Tmem74* mice (**h**, n=11 in each group) and the number of buried marbles (**i,** n=12 in each group). **j-m** The interaction time (**j**) and social preference index (**k**) in all groups during phase 2, and the interaction time (**l**) and social novelty index (**m**) during phase 3 from three-chamber test (n=11 in each group). **n**, **o** Representative heatmaps and time in central zone (**n**), the entries of central zone (**o**) in the open field test (n=11 in each group). **p-r** Representative heatmaps and entries of open arms in the elevated plus maze (**p**), the time in open arms (**q**) and the exploring time in closed arms (**r**) (n=11 in each group).

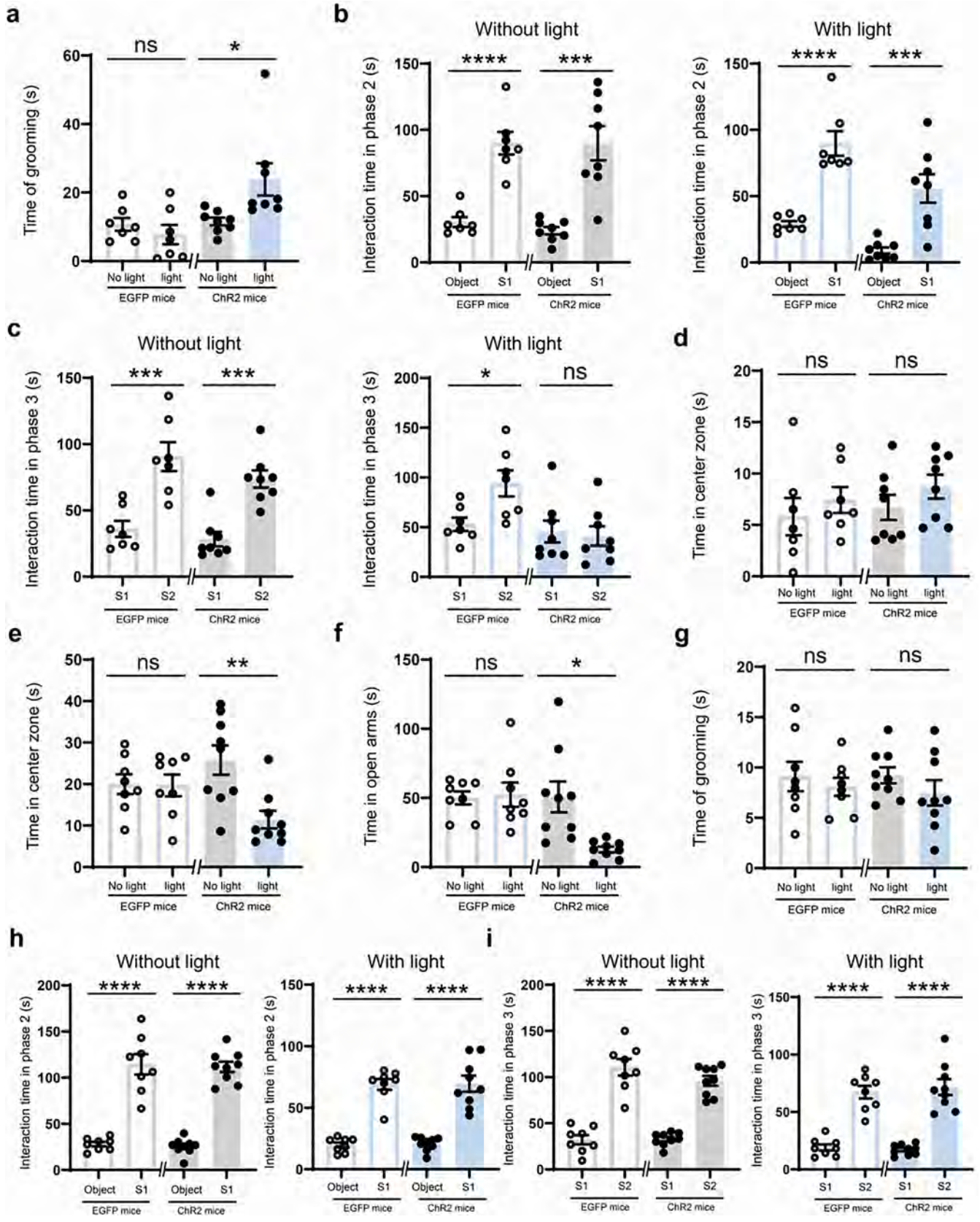

**Fig 2. Optogenetic activation of PL-dSTR or PL-BLA led to autistic-like behaviors or anxiety-like behaviors respectively. a-d** ASD related and anxiety behviors were performed after optogenetic activation of PL-dSTR or not. CaMKIIα-Cre mice+AAV-DIO-EGFP: n=7; CaMKIIα-Cre mice+AAV-DIO-ChR2-EGFP: n=8. **e-i** Anxiety behaviors and ASD related were performed after optogenetic activation of PL- BLA or not. CaMKIIα-Cre mice+AAV-DIO-EGFP: n=8; CaMKIIα-Cre mice+AAV-DIO-ChR2-EGFP: n=9.

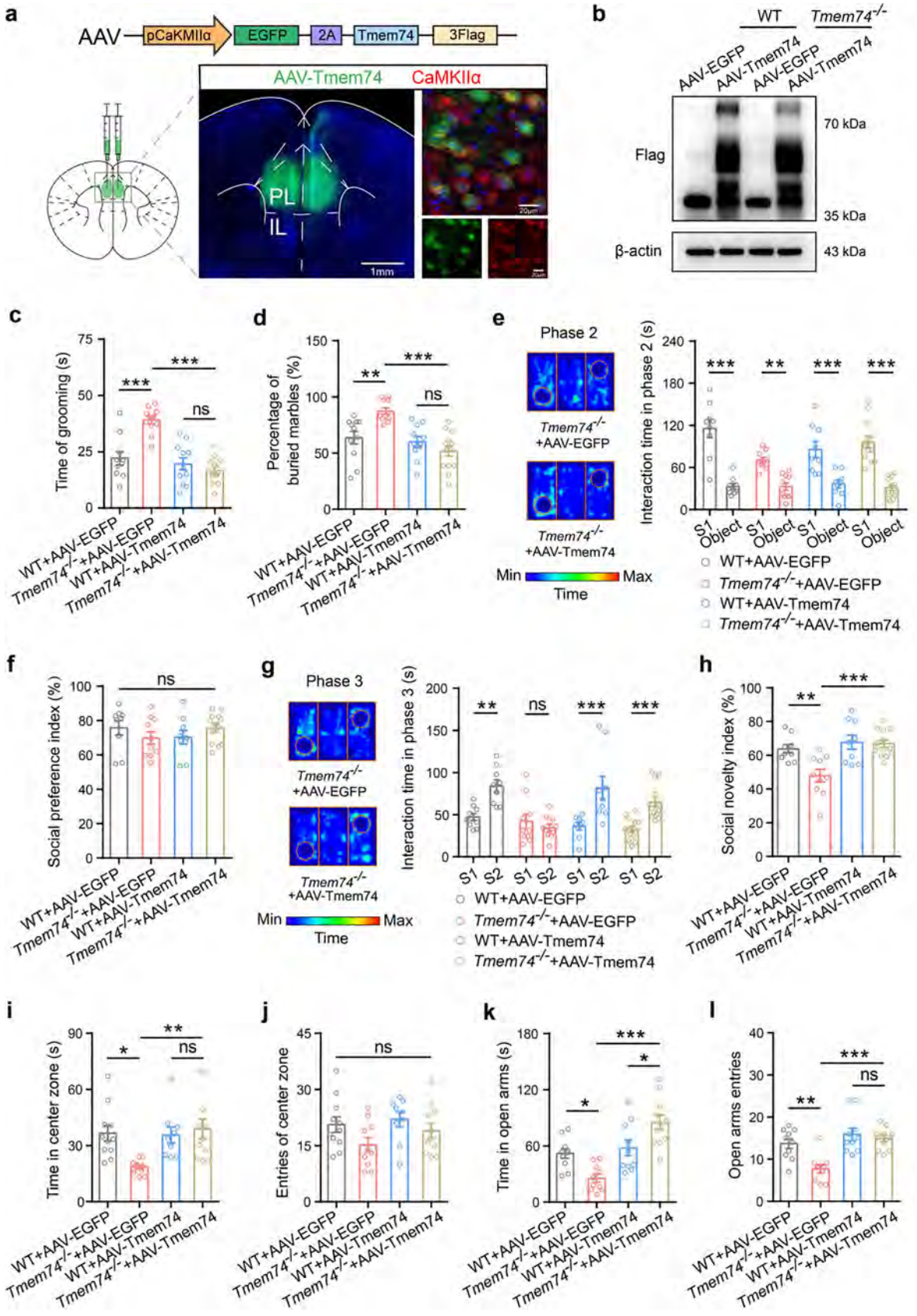

**Fig. 3 Overexpression of TMEM74 in PL rescues social deficits and anxiety-like behaviors. c-h** Quantification of the grooming time (**c**), the percentage of buried marble (**d**), the interaction time (**e**) and the sociability preference index (**f**) with S1 mouse in the phase 2, and the time spent interacting (**g**) and social novelty index (**h**) with novel S2 in the phase 3 of three-chamber tests after AAV-EGFP or AAV-TMEM74 injection to PL. **i**, **j** Quantification of the time in central zone (**i**) and the entries of central zone (**j**) in the open field test. **k**, **l** Quantification of the time spent in open arms (**k**) and number of entries to open arms (**l**) in the elevated plus maze. n=9-11 WT+AAV-EGFP mice, n=10-12 *Tmem74*$^{-/-}$+AAV-EGFP mice, n=9-11 WT+AAV-Tmem74 mice, n=11-13 *Tmem74*$^{-/-}$+AAV-Tmem74 mice.

## OC134 | Anti-Inflammatory And Neuroprotective Effects Of Oleoylethanolamide In A Rat Model Of Diet-Induced Obesity

**Nisha Zahid**
*Sapienza University Of Rome*

**Introduction**

A well-described feature of obesity is chronic, unresolved tissue inflammation and it is associated with a cluster of central and peripheral alterations including neuroinflammation and modification in the integrity and functionality of the blood brain barrier (BBB)[1]. In this scenario, oleoylethanolamde (OEA), a naturally occurring bioactive lipid, has received great attention for its biological properties. It has been demonstrated that OEA exerts a plethora of protective effects including anti-obesity, anti-inflammatory, and antioxidant properties thus supporting its potential use for the treatment of obesity and eating-related disorders [2–4]. Hence, by using a rat model of diet-induced obesity (DIO), the aim of the present study was to evaluate whether rats with an obese phenotype showed neuroinflammation and modification in the integrity and functionality of the BBB and subsequently whether the chronic peripheral administration of OEA (10 mg/kg) might ameliorate such alterations.

**Methods**

In this study we used a rat model of DIO based on exposure for 11 weeks to a high-fat diet (HFD:60% of the kcal from fats); the control group received a low-fat diet (LFD:10% of the kcal from fats). Starting from the 12th week, all the animals were chronically treated for 2 weeks with either VEH or OEA (10 mg/kg i.p.). Brains collected from all animals groups were used in immunohistochemistry and immunofluorescence experiments to evaluate: 1) GFAP expression levels as a marker of neuroinflammation; 2) vimentin (VIM) and zona occludens (ZO)-1 expression levels as proteins of the BBB; 3) doublecortin (DCX) as a marker of neurogenesis.

**Results**

Our results revealed that, in HFD-fed animals, OEA administration completely reverted the expression of GFAP to the level observed in VEH-treated animals. Moreover, OEA treatment modulated the expression of VIM and ZO-1, key proteins involved in the integrity and functionality of BBB. Finally, OEA treatment increased the number of DCX-positive neurons in both lean and obese rats

**Conclusions**

Taken together, our data demonstrated that OEA is reducing food intake and body weight gain accompanied by decreased neuroinflammation and improved neuroprotection. Hence, OEA has strong potential to be used as a pharmacological target to treat obesity and its related alterations.

**Statistical Analysis:**

All data were expressed as mean ± SEM. Regarding the data of FI, BWG, GFAP, VIM, ZO-1, DCX, were analyzed with a two-way ANOVA for repeated measures and the Bonferroni's test was used as post-hoc analysis for multiple comparisons (IBM SPSS, version 22, IBM Analytics).

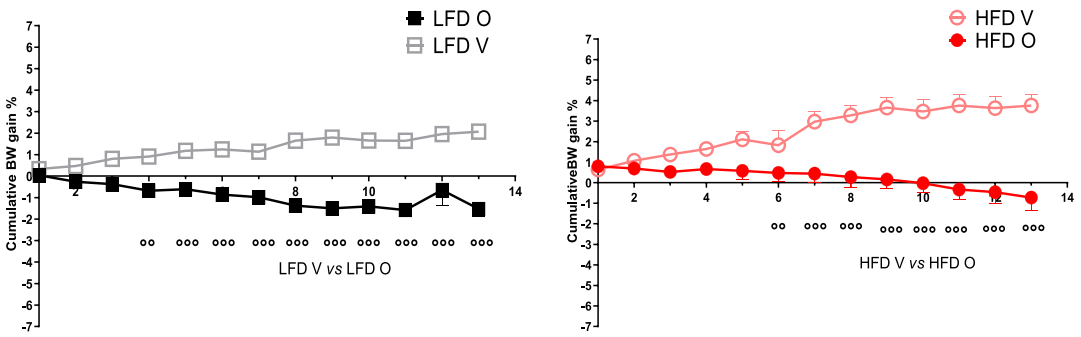


**FIGURE 1** (A): Time course of the body weight gain (BW gain) of animals exposed to LFD and HFD diet and treated with either VEH or OEA (10 mg/kg, i.p.)

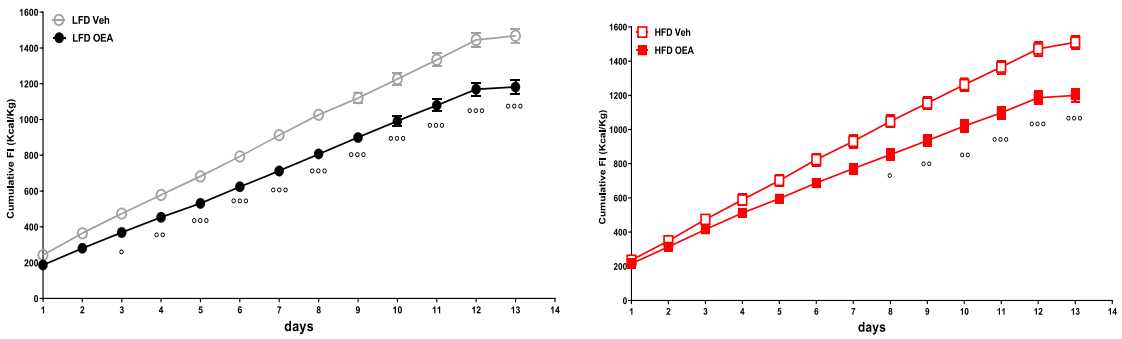


**FIGURE 1** (B): Time course of the caloric intake (FI) of animals exposed to LFD and HFD diet and treated with either VEH or OEA (10 mg/kg, i.p.)

BJP BRITISH PHARMACOLOGICAL SOCIETY



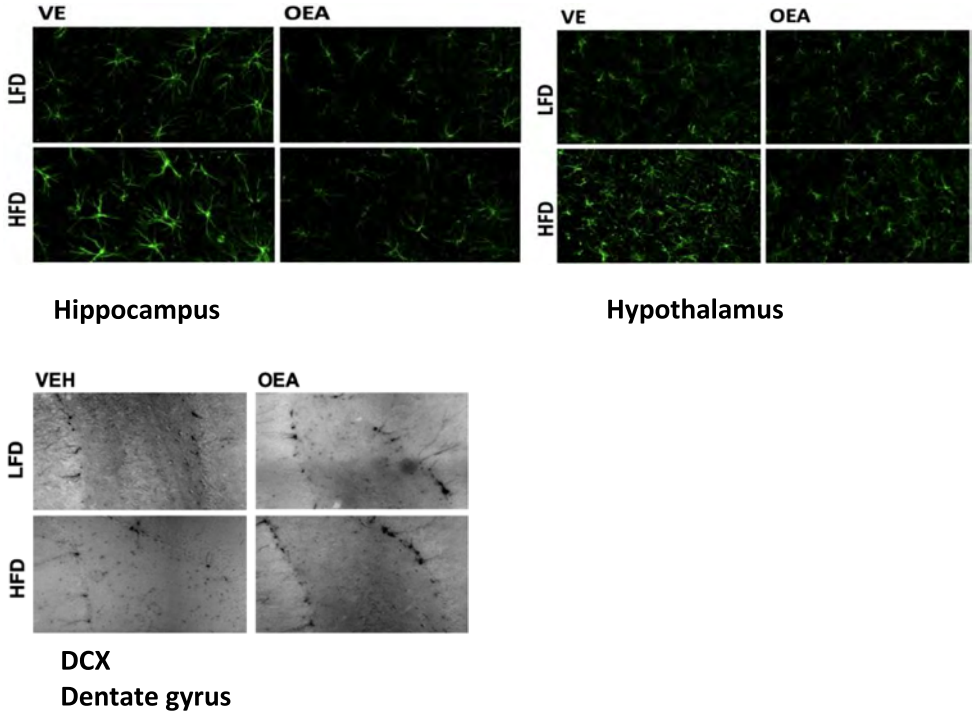


**FIGURE 2** OEA affects GFAP expression and DCX-positive neurons

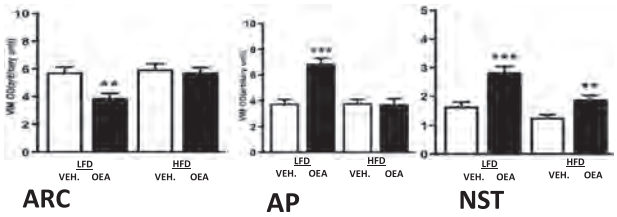


**FIGURE 3** OEA affects the expression of Vimentin i.e. protein involved in the regulation of BBB

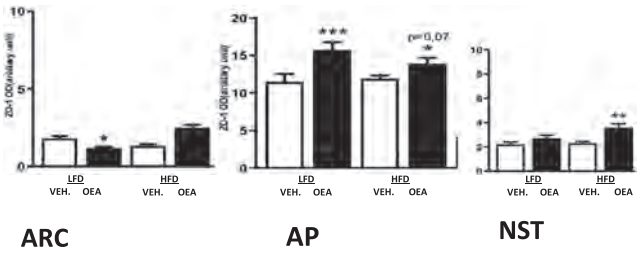


**FIGURE 4** OEA affects the expression of Zona Occludens i.e. protein involved in the regulation of BBB

**References**

1. https://doi.org/10.1038/s41574-019-0286-3
2. https://doi.org/10.3389/fphar.2015.00137
3. https://doi.org/10.1111/jnc.13848
4. doi:10.1038/s41386-020-0686-z.

LFD HFD

# OC146 | Human induced pluripotent stem cell-derived repair of the Parkinsonian rat brain is enhanced by delivery of cells in a neurotrophin-enriched hydrogel

**Rachel Kelly[4]; Sarah Jarrin[1]; Tommy Patton[1]; Giulia Comini[1]; Kaushik Narasimhan[1]; Abhay Pandit[2]; Nicola Drummond[4]; Tilo Kunath[4]; Eilís Dowd[1]**

*[1]Pharmacology & Therapeutics, University Of Galway; [2]CÚRAM SFI Centre for Research in Medical Devices, University of Galway; [3]Centre for Regenerative Medicine, University of Edinburgh; [4]Danish Research Institute of Translational Neuroscience (DANDRITE) and Department of Biomedicine, Aarhus University*

**Introduction**

Although induced pluripotent stem cell (iPSC)-derived brain repair for Parkinson's has considerable reparative potential, its therapeutic benefit is limited by poor graft survival and maturation in the brain. This is due to the necessity for lifting iPSC-derived dopaminergic progenitors from their neurotrophin-enriched cell culture environment and transplanting them into the neurotrophin-depleted adult Parkinsonian brain. We have shown that collagen hydrogels can be used to provide a neurotrophin reservoir in the brain thereby providing a more favourable microenvironment to implanted cells. Thus, the aim of this study was to determine if this neurotrophin-enriched hydrogel [1,2] could improve the survival and maturation of iPSC-derived dopaminergic progenitors in the Parkinsonian rat brain.

**Methods**

Female athymic rats were administered 6-hydroxydopamine via stereotaxic infusion into the medial forebrain bundle (12 µg in 3 µl; unilaterally; isofluorane anaesthesia) to induce the nigrostriatal degeneration associated with Parkinsonism. Three weeks later, rats were randomly divided into 4 groups (n=6-7 rats per group) for transplantation with human iPSC-derived dopaminergic progenitors (300,000 cells at Day 16 of dopaminergic differentiation) either alone, with neurotrophin enrichment (GDNF: 500 ng/transplant; BDNF: 1000 ng/transplant), in a collagen hydrogel (5 mg/ml collagen crosslinked with 4 mg/ml 4-arm-StarPEG), or in a neurotrophin-enriched collagen hydrogel (6 µl/transplant for all). Rats were sacrificed 20 weeks after transplantation for blinded post-mortem evaluation of graft survival (human cytoplasmic (STEM121) and nuclear (HuNu) immunostaining) and dopaminergic maturation (tyrosine hydroxylase (TH) immunostaining).

**Results**

Immunohistochemical staining for human cytoplasm, human nuclei and dopaminergic neurons in the rat striatum clearly showed surviving and maturing human grafts in all groups (Fig. 1A). However, the grafts were small and compact when the iPSC-derived dopaminergic progenitors were transplanted alone, but appeared much larger and more dispersed when they were transplanted in the neurotrophin-enriched hydrogel. Quantification (Fig. 1B) of STEM121-immunopositive graft volume (Group, $F(3, 22) = 10.6$, $P<0.001$), HuNu-immunopositive nuclear counts (Group, $F(3, 22) = 8.47$, $P<0.001$) and TH-immunopositive cell counts (Group, $F(3, 22) = 33.11$, $P<0.0001$) confirmed the dramatic beneficial effect of the neurotrophin-enriched hydrogel on graft survival and dopaminergic maturation.

**Conclusions**

Transplantation of human iPSC-derived progenitors in a neurotrophin-enriched collagen hydrogel dramatically improved graft survival and dopaminergic maturation in the Parkinsonian rat brain. The data strongly supports further investigation of this biomaterial matrix for improving the outcome of iPSC-derived brain repair in Parkinson's disease.

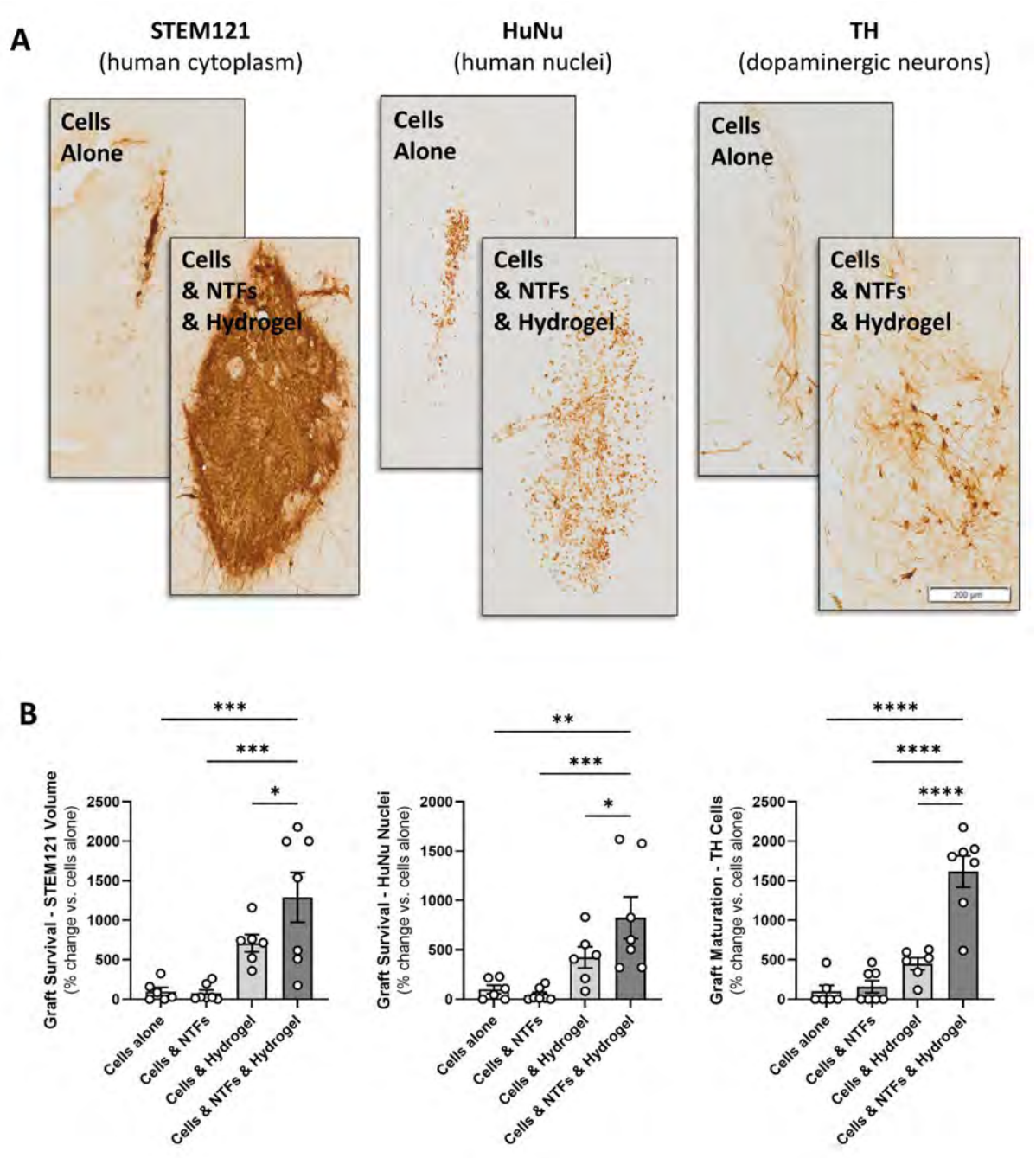


**Fig. 1 Impact of the neurotrophin-enriched hydrogel on human iPSC-derived dopaminergic progenitor survival and maturation in the Parkinsonian rat brain.** A) STEM121 (human cytoplasm), HuNu (human nuclei) and TH (dopaminergic neurons) revealed surviving and maturing human grafts in all groups with much larger grafts visible when the cells were transplanted in the neurotrophin-enriched hydrogel. B) Quantification of graft survival (STEM121 graft volume and HuNu nuclear counts) and maturation (TH cell counts) confirmed the beneficial effect of the neurotrophin-enriched hydrogel with ~10x enhancement of survival and ~15x enhancement of maturation. Data are mean ± SEM with n=6/7 rats per group. **P*<0.05, ***P*<0.01, ****P*<0.001, *****P*<0.0001 by 1-way ANOVA with *post hoc* Newman Keuls. NTFs: Neurotrophins. Scale bar: 200 μm.

**References**

1. Moriarty et al., 2019. Eur J Neurosci. 49:487-496
2. Moriarty et al., 2017. Sci. Rep. 7:16033.

# OC163 | The binding kinetics of fentanyls and nitazenes at the u opioid receptor

**Ms Norah Alhosan**
*University Of Bristol*

## Introduction

Fentanyls and nitazenes are potent μ opioid receptor (MOR) agonists. They are reported to be harder to reverse by naloxone in overdose cases and this has been ascribed to their high affinity and potency [1]. However, according to receptor theory, a competitive antagonist should be equally effective in reversing all agonists acting at the same receptor. We studied the ability of naloxone to reverse the response of a range of fentanyls and nitazenes and measured the apparent dissociation half-time of each agonist. We examined the correlation between the ability of naloxone to reverse each agonist with their lipophilicity, and apparent dissociation half-time. Moreover, we investigated the G protein and arrestin signalling bias profile of these ligands and how bias behaviour may correlate to the dissociation rate.

## Methods

We used membrane potential dye to measure membrane hyperpolarising responses to fentanyls and nitazenes in AtT20 cells expressing the human MOR in vitro and compared them to the prototypic MOR agonists DAMGO and morphine. Reversal experiments were designed to resemble the overdose situation whereby the agonist was added first before the antagonist. A sub-maximal concentration (EC75) of each agonist was added and the response was allowed to reach equilibrium whereupon naloxone was added. For the bias studies, agonist-induced G protein activation and arrestin translocation to the MOR were measured by BRET2 in HEK293 cells transiently transfected.

## Results

The IC50 values for naloxone are shown in Table 1. We observed that alfentanil, fentanyl, DAMGO and morphine dissociated rapidly from the receptor (with t1/2 values close to the lower limit of the assay procedure). However, other agonists dissociated more slowly from MOR with a rank order of sufentanil < etonitazene ≤ isotonitazene < ohmefentanyl < carfentanil. Susceptibility to naloxone reversal was poorly correlated with the lipophilicity of the agonist (R2=0.23) (Figure 1). However, the rate of agonist unbinding from MOR was highly correlated with naloxone reversal (R2=0.99) (Figure 2). We are currently investigating the possible correlation between the rate of unbinding of the agonists from MOR and their bias between G protein activation and arrestin recruitment.

## Conclusions

While fentanyls and nitazenes are all lipophilic drugs, their lipophilicity profile did not predict their naloxone reversibility. In contrast, their rate of dissociation from the receptor did correlate with their naloxone reversibility.

**Table 1**

| Drug ($EC_{75}$) | Naloxone $IC_{50}$ (nM) | $t_{1/2}$ of agonist unbinding (secs)* |
|---|---|---|
| **Fentanyl (15nM)** | 3.2 | 6.4 |
| **Morphine (200nM)** | 3.7 | 6.3 |
| **DAMGO (20nM)** | 3.9 | 6.5 |
| **Alfentanil (50nM)** | 6.4 | 6.5 |
| **Isotonitazene (60nM)** | 18.6 | 30 |
| **Etonitazene (12nM)** | 21.2 | 28 |
| **Sufentanil (10nM)** | 22.2 | 16 |
| **Ohmefentanyl (5nM)** | 32.6 | 33 |
| **Carfentanil (5nM)** | 118.2 | 74 |

***Measured as the decay in response following the addition of naloxone (10 mM)**

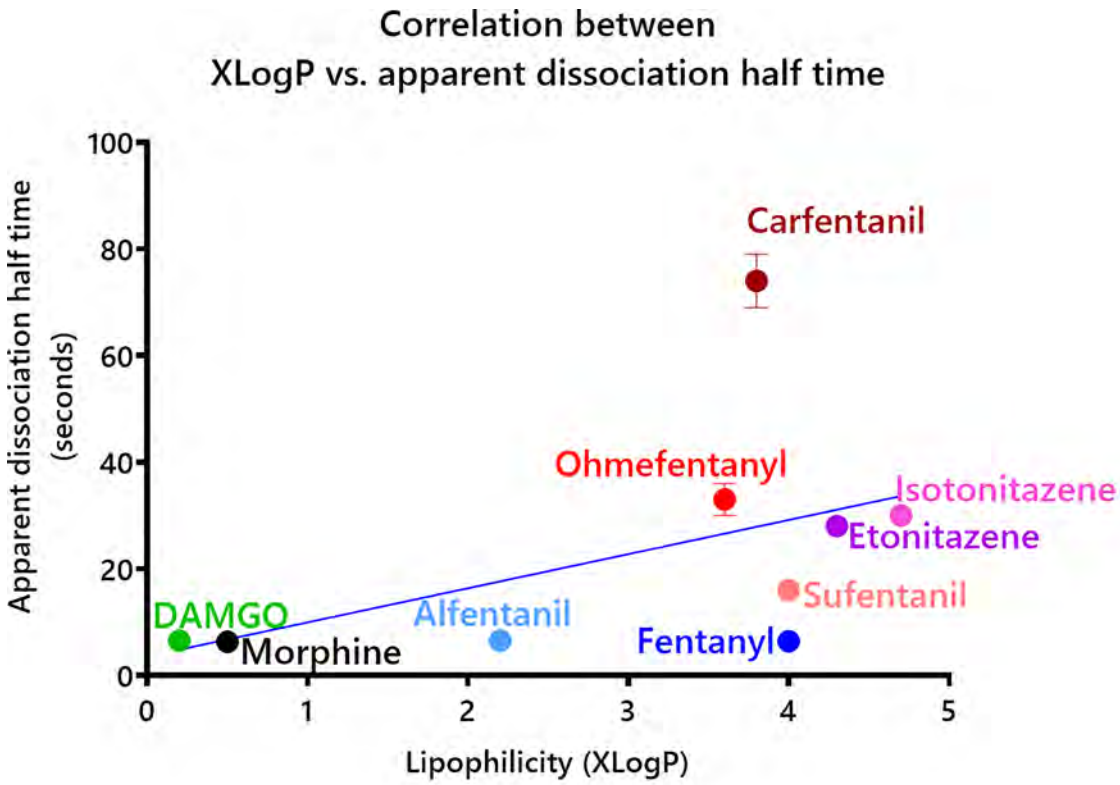


*Figure 1 Correlation between XLogP and apparent dissociation half time*

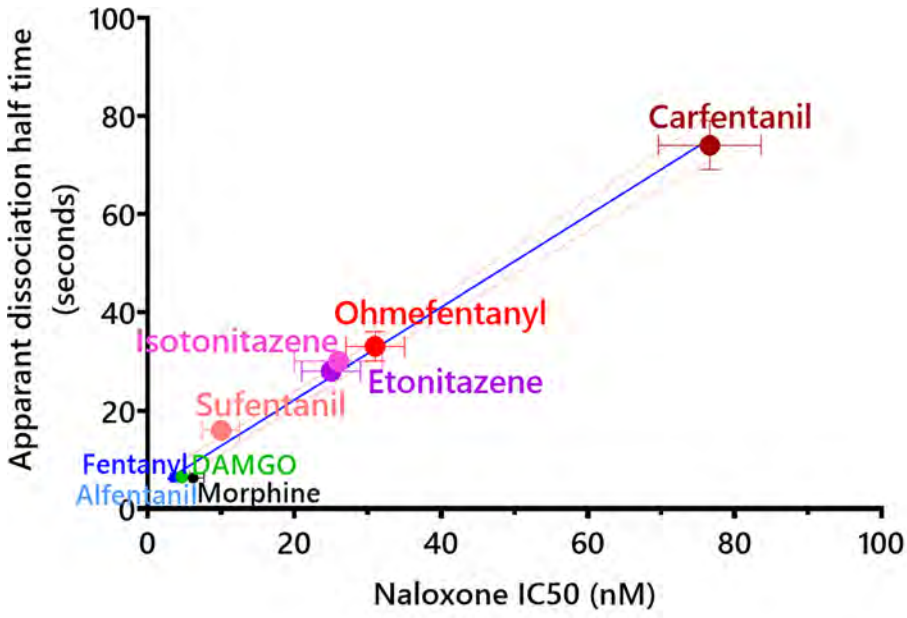


*Figure 2 Correlation between naloxone $IC_{50}$ and apparent dissociation half time*

**Reference**

1. Moe J, Godwin J, Purssell R, et al. Naloxone dosing in the era of ultra-potent opioid overdoses: a systematic review. CJEM. 2020;22(2):178-186. https://doi.org/10.1017/cem.2019.471

## OC165 | Autism spectrum disorders: sex matters in a mouse model of idiopathic autism

**Luigia Trabace; Maria Bove**
*University of Foggia*

**Introduction**

Autism spectrum disorders (ASD) are highly heterogeneous neurodevelopmental diseases. Epidemiological studies reported that males are three times more frequently diagnosed with ASD than females. However, recent studies hypothesize that females' low incidence might be underestimated due to standard clinical measures of ASD behavioural symptoms, mostly studied in males. As regarding ASD aetiopathogenesis, the mechanisms underpinning behavioural symptoms have not been fully elucidated yet. Recently, it has been reported that oxidative stress and oxytocin alterations might be crucially implicated in ASD onset and development. Indeed, ASD patients are characterized by lower plasma oxytocin and its ectoenzyme regulator CD38, together with increased oxidative stress. Thus, antioxidant treatment might represent a new therapeutic strategy to improve ASD behavioural deficits. Among antioxidant compounds, B-carotene, a non-toxic molecule from the retinoid family, is also a potent CD38 inducer.

**Methods**

In the present study, we investigated possible behavioural sex-related differences by using a mouse model of idiopathic autism, the BTBR inbred strain. Moreover, we evaluated possible preventive effects of B-carotene supplementation (16mg/kg in seeds oil) in BTBR offspring. Animals were exposed to behavioural tests related to ASD core symptoms, i.e. Marble Burying, Grooming behaviour and Hole Board tests for stereotyped repertoire and Social Interaction test for social deficits. Group size was between 8-12 for each experiment. Statistical significance was determined using a Two-Way ANOVA followed by Tukey's post-hoc test on raw data.

**Results**

Our results showed that BTBR females did not display the same behavioural patterns for repetitive behaviours compared to the male counterpart ($P<0.0001$ BTBR male vs Ctrl male and vs BTBR female for Marble Burying, $P<0.05$ BTBR male vs Ctrl male for grooming), but they showed the same social dysfunctions ($P<0.0001$ BTBR vs Ctrl male and $P<0.01$ BTBR vs Ctrl female for duration, $P<0.001$ BTBR vs Ctrl male and $P<0.05$ BTBR vs Ctrl female for frequency). As regarding B-carotene supplementation, such treatment, administered during pregnancy in BTBR dams, was able to ameliorate stereotyped repertoire in male offspring ($P<0.05$ B-carotene vs Ctrl for Marble Burying, $P<0.001$ B-carotene vs Ctrl for grooming) and to improve social interactions in both male and female offspring ($P<0.01$ B-carotene vs Ctrl male and $P<0.0001$ B-carotene vs Ctrl female).

**Conclusions**

Overall, our study suggest that BTBR mice display sex specific stereotyped repertoire, pointing toward an urgent need of a deeper evaluation in females, and that B-carotene administration during pregnancy might represent a useful approach to prevent/ameliorate ASD behavioural dysfunctions.

## OC166 | Resilient and vulnerable rats to acute foot shock stress show different glial cell responses: possible rescue of pathological alterations by a single ketamine administration

**Marta Valenza[1]; Roberta Facchinetti[1]; Marco Milanese[2]; Laura Musazzi[3]; Giambattista Bonanno[2]; Luca Steardo[1]; Tiziana Bonifacino[2]; Caterina Scuderi[1]**
*[1]Sapienza University of Rome; [2]University of Genoa; [3]University of Milano-Bicocca*

**Introduction**

Acute traumatic experiences trigger neurobiological changes in the brain. In vulnerable subjects, such alterations persist and lead to the development of psychiatric conditions [1]. The alterations studied so far mainly pertain to neurons [1,2], neglecting glial cells, which instead play key roles in brain homeostasis [3]. By using a validated animal model, we studied the differential impact of traumatic stress on cortical glial cells of resilient (RES) and vulnerable (VUL) rats [2]. To test a possible translationally relevant rescue strategy, we administered the rapid antidepressant ketamine 24h after stress and analyzed rat cortices 24h later.

**Methods**

Adult Sprague-Dawley rats were exposed to a single footshock stress (FS, 40 min-intermittent, 0.8mA [2]). Rats showing anhedonia, measured by reduction in 1h-sucrose (1%) intake ≥25% compared with baseline (BL: 4 week-mean intake before FS), were identified as VUL, while rats showing ≤10% change were considered RES. Markers of both glial cells and neurons morphology and functions as well as of neuroinflammation were

studied in cortices (n=4-6/group, collected 24h or 48h after FS) by RT-PCR, western blotting and immunofluorescence, and analyzed by one-way ANOVA followed by Tukey's test. Ketamine (10 mg/kg; i.p.)- and vehicle-treated rats were compared by Student's t test; p≤0.05 was considered significant.

**Results**

VUL displayed robust and prolonged anhedonic-like behavior after FS. Astrocytes were reactive 24h after FS, without changes in the dendritic marker MAP 2. Reactive astrocytes and microglia and elevation in parameters of inflammation were observed 48h after FS selectively in VUL with activation of the NFkB pathway. VUL also showed reduced MAP 2 expression. Ketamine in VUL dampened microglia reactivity and neuroinflammation, reducing activation of the NFkB pathway , also rescuing MAP 2 expression. Ketamine did not affect such parameters in RES.

**Conclusions**

This study suggests that acute stress affects glial cells and that their responses are different in RES and VUL, as well as that Ketamine could be beneficial to turn off the pathological process triggered by stress. Data collected lay the foundation for future studies with diagnostic and therapeutic implications having glial cells as target.

**References**

1. Sanacora G, Yan Z, Popoli M. The stressed synapse 2.0. Nat Rev Neurosci. 2022;23(2):86-103.

2. Sala N, Paoli C, Bonifacino T, et al. Acute ketamine facilitates fear memory extinction in a rat model of PTSD restoring glutamatergic alterations in the prefrontal cortex. Front Pharmacol. 2022;13:759626.

3. Scuderi C, Verkhratsky A, Parpura V, Li B. Neuroglia in Psychiatric Disorders. Adv Neurobiol. 2021;26:3-19.

## OC191 | Co-ultramicronized palmitoylethanolamide/luteolin restores the astrocyte-oligodendrocyte cross-talk required for myelination via peroxisome proliferator-activated receptor-α in an in vitro model of Alzheimer's disease

**Roberta Facchinetti[1]; Marta Valenza[1]; Chiara Gomiero[2]; Luca Steardo[1]; Patrizia Campolongo[1]; Caterina Scuderi[1]**
*[1]Sapienza University of Rome; [2]Epitech Research Group*

**Introduction**

The astrocyte/oligodendrocyte crosstalk is necessary for myelin sheath formation [1]. In Alzheimer's disease (AD), the deposition of beta-amyloid (Aβ) has been linked to astrogliosis but also changes in oligodendrocyte maturation. However, very little is known about the molecular mechanisms involved. To contribute to filling this gap, we investigated the astrocyte/oligodendrocyte crosstalk in an in vitro model of Aβ1–42 toxicity and tested the effect of the anti-inflammatory and neuroprotective composite palmitoylethanolamide and luteolin (co-ultra PEALut), known to engage the peroxisome proliferator-activated receptor (PPAR)-α.

**Methods**

All animal procedures were performed in agreement with the European Parliament directive 2010/63/EU. After isolation from the brain of 0-2 PND female Sprague Dawley rat pups (6 pups/experimental group) [2], primary OPCs were co-cultured with astrocytes allowing secreted soluble factors to diffuse while preventing physical contact. Using RT-qPCR and immunofluorescence, we tested the possible beneficial effect of co-ultra PEALut 3 μM (dissolved in Pluronic F-68) treatment in counteracting Aβ1–42 1 μM (dissolved in water)-induced toxicity by studying the modifications of the astrocytic functions and the maturation and morphology of co-cultured oligodendrocytes. The involvement of PPAR-α was verified by using GW6471 3 μM (dissolved in DMSO), a selective PPAR-α antagonist. Data were analyzed with one-way analysis of variance with Student Newman Keuls post-hoc for multiple comparisons.

**Results**

Our results show that Aβ1-42 triggers astrocyte reactivity and inflammation and reduces the levels of fibroblast growth factor (FGF)2 and transforming growth factor (TGF)-β (Table 1). The maturation of co-cultured oligodendrocytes increases after Aβ1-42 challenge but differentiated oligodendrocytes show a lower cell surface area and fewer arborizations with respect to control cells (Table 2). Co-ultra PEALut counteracts the Aβ1-42-induced inflammation and astrocyte reactivity (Table 1), preserving the morphology of co-cultured oligodendrocytes (Table 2) through a mechanism that in some cases involves PPAR-α (Table 1 and 2).

**Conclusions**

This study provides the first evidence of the negative effects exerted by Aβ1-42 on the astrocyte/oligodendrocyte crosstalk and discloses a never explored co-ultra PEALut ability in restoring oligodendrocyte homeostasis.

**Table 1. Mean ± SEM of RT-qPCR experiments performed on astrocytes (N=6).**

| Marker | Experimental group (Mean ± SEM) | | | |
|---|---|---|---|---|
| | CTRL | $A\beta_{1-42}$ | Co-ultraPEALut+ $A\beta_{1-42}$ | Co-ultraPEALut+ $A\beta_{1-42}$+GW6471 |
| GFAP | 1 ± 0,13 | 6,54 ± 2,13$^{***}$ | 0,32 ± 0,02$^{°°°}$ | 0,72 ± 0,18 |
| S100B | 1 ± 0,25 | 24,35 ± 4,88$^{***}$ | 0,59 ± 0,03$^{°°°}$ | 0,64 ± 0,07 |
| FGF2 | 1 ± 0,03 | 0,24 ± 0,004$^{**}$ | 0,67 ± 0,13$^{°}$ | 0,55 ± 0,05 |
| TGF-β | 1 ± 0,10 | 0,18 ± 0,02$^{**}$ | 0,76 ± 0,23$^{°}$ | 0,93 ± 0,03 |
| IL-6 | 1 ± 0,06 | 3,04 ± 0,15$^{***}$ | 0,63 ± 0,08$^{°°°}$ | 2,72 ± 0,24$^{\$\$\$}$ |
| IL-1β | 1 ± 0,10 | 1,52 ± 0,06$^{***}$ | 0,76 ± 0,10$^{°°}$ | 1,34 ± 0,16$^{\$\$}$ |

GFAP: glial fibrillary acidic protein; FGF: fibroblast growth factor; TGF: transforming growth factor; IL: interleukin

$^{*}$ $p < 0,05$ vs CTRL; $^{°}$ $p < 0,05$ vs $A\beta_{1-42}$; $^{\$}$ $p < 0,05$ vs co-ultraPEALut + $A\beta_{1-42}$

**Table 2. Mean ± SEM of immunofluorescence experiments performed on oligodendrocytes (N=6).**

| Outcome | Experimental group (Mean ± SEM) | | | |
|---|---|---|---|---|
| | CTRL | $A\beta_{1-42}$ | Co-ultraPEALut+ $A\beta_{1-42}$ | Co-ultraPEALut+ $A\beta_{1-42}$+GW6471 |
| $MBP^{+}/Olig2^{+}$ | 100 ± 2,30 | 109,74 ± 0,94$^{*}$ | 102,22 ± 1,77$^{°}$ | 105,84 ± 1,47 |
| Total cell surface | 409,13 ± 21,62 | 310,64 ± 14,80$^{*}$ | 390,52 ± 29,56$^{°}$ | 370,06 ± 20,30 |
| Max intersections | 59,00 ± 2,46 | 48,00 ± 1,88$^{**}$ | 66,00 ± 4,16$^{°°}$ | 50,00 ± 2,04$^{\$\$}$ |
| Sum of intersections | 167,17 ± 9,24 | 129,98 ± 7,72$^{*}$ | 186,85 ± 11,08$^{°°}$ | 145,17 ± 9,18$^{\$}$ |
| Mean of intersections | 44,98 ± 1,95 | 34,22 ± 1,58$^{***}$ | 47,13 ± 1,87$^{°°°}$ | 35,19 ± 1,46$^{\$\$\$}$ |

MBP: myelin basic protein

$^{*}$ $p < 0,05$ vs CTRL; $^{°}$ $p < 0,05$ vs $A\beta_{1-42}$; $^{\$}$ $p < 0,05$ vs co-ultraPEALut + $A\beta_{1-42}$

**References**

1. Tognatta R, Karl MT, Fyffe-Maricich SL, Popratiloff A, Garrison ED, Schenck JK, Abu-Rub M, Miller RH (2020) Astrocytes are required for oligodendrocyte survival and maintenance of myelin compaction and integrity. Front Cell Neurosci. 14:74.

2. Barbierato M, Facci L, Marinelli C, Zusso M, Argentini C, Skaper SD, Giusti P (2015) Co-ultramicronized palmitoylethanolamide/luteolin promotes the maturation of oligodendrocyte precursor cells. Sci Rep. 5:16676.

# P0196 | The effect of trans-resveratrol against NMDA-induced retinal nitrosative stress involves adenosine A1 receptors

**Afiqq Aiman Abd Ghapor; Nurul Alimah Abdul Nasir; Norhafiza Razali; Igor Iezhitsa; Renu Agarwal**
*International Medical University*

## Introduction

Glaucoma, a neurodegenerative condition, is the leading cause of irreversible visual loss globally [1]. It is characterized by the retinal ganglion cells (RGCs) apoptosis associated with glutamate-induced excitotoxicity and a suppressed activity of adenosine A1 receptors (A1AR) [2]. Furthermore, retinal nitrosative stress resulting from increased expression of inducible nitric oxide synthase (iNOS) contributes to excitotoxicity-induced RGC apoptosis. Trans-resveratrol (TR), a polyphenol, is known to increase the A1AR activity and provide neuroprotection [3]. We investigated if TR suppresses N-methyl D aspartate (NMDA)-induced retinal nitrosative stress by activating A1AR in rats.

## Methods

Four groups of thirty-two Sprague Dawley rats were treated intravitreally in one of the randomly chosen eyes. Group 1 received vehicle; Group 2 was treated with NMDA (160 nmol); Group 3 received pre-treatment with TR (4 nmol) followed by NMDA and Group 4 was pretreated with TR (4 nmol) and DPCPX (adenosine A1 receptor antagonist, 8 nmol) followed by NMDA. Rats were euthanized 7 days later and retinal 3-nitrotyrosine (3-NT) and iNOS protein expression were measured using ELISA.

## Results

The NMDA-treated group 2 showed higher retinal 3NT levels compared to vehicle-treated group 1 (7.39 folds, $p<0.001$). Pretreatment with TR in group 3 lowered the retinal 3-NT levels compared to group 2 (2.93 folds, $p<0.001$). Notably, addition of DPCPX abolished the effect of TR pre-treatment as the retinal 3-NT level in group 4 was 2.47 folds greater than group 3 ($p<0.001$) and 6.38 folds greater than group 1 ($p<0.001$). Accordingly, retinal iNOS expression in group 3 was 14.7 folds lower than group 2 ($p<0.001$) while the same in group 4 was 6.98- and 17.09 folds higher than group 3 and 1, respectively ($p<0.001$). (Figure 1)

## Conclusions

TR lowers NMDA-induced retinal nitrosative stress in rats, which could at least partially be attributed to activation of A1AR.

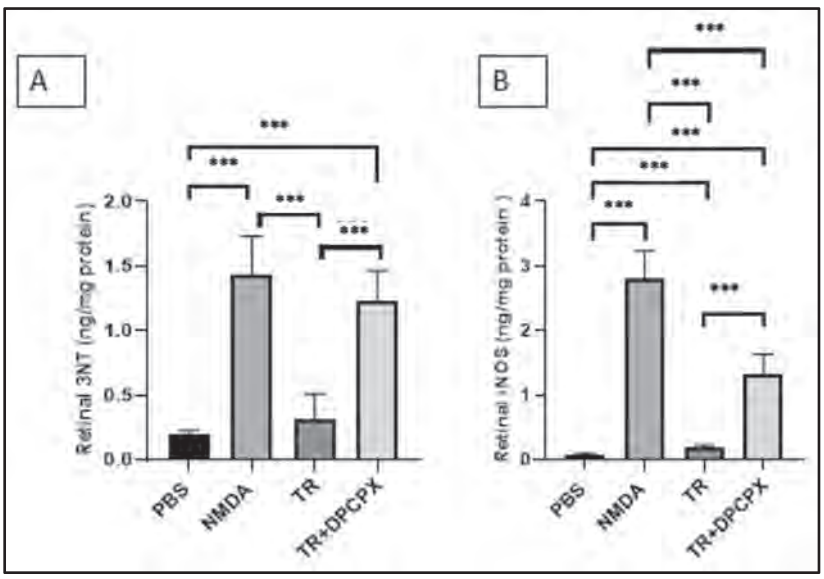


**FIGURE 1** The effect of intravitreal injection of TR in the presence and absence of DPCPX against NMDA induced retinal nitrosative stress in rats. (A) Retinal 3-NT contents (b) Retinal iNOS expression. *** $p<0.001$

## References

1. Zhang N, Wang JLY, Jiang B. Prevalence of primary open angle glaucoma in the last 20 years: a meta-analysis and systematic review. Scientific Reports. 2021;11(1):1–12. https://doi.org/10.1038/s41598-021-92971-w

2. Arfuzir NNN, Agarwal R, Iezhitsa I, et al. Effect of magnesium acetyltaurate and taurine on endothelin1-induced retinal nitrosative stress in rats. Curr Eye Res. 2018;43(8):1032-1040. https://doi.org/10.1080/02713683.2018.1467933